ORNL/TM-2003/217

OAK RIDGE
NATIONAL LABORATORY

MANAGED BY UT-BATTELLE
FOR THE DEPARTMENT OF ENERGY

Determination of the Applicability of Hydrostatic Proof Testing for Demonstrating Integrity of HFIR Primary-System Piping, Vessel, and Related Components

December 2003

R. D. Cheverton
Consultant

J. R. Inger
Engineer

Central Research Library
MS-6208; Bldg. 4500N

UT-BATTELLE
ORNL-27 (2-03)

DOCUMENT AVAILABILITY

Reports produced after January 1, 1996, are generally available free via the U.S. Department of Energy (DOE) Information Bridge:

Web site: http://www.osti.gov/bridge

Reports produced before January 1, 1996, may be purchased by members of the public from the following source:

National Technical Information Service
5285 Port Royal Road
Springfield, VA 22161
Telephone: 703-605-6000 (1-800-553-6847)
TDD: 703-487-4639
Fax: 703-605-6900
E-mail: info@ntis.fedworld.gov
Web site: http://www.ntis.gov/support/ordernowabout.htm

Reports are available to DOE employees, DOE contractors, Energy Technology Data Exchange (ETDE) representatives, and International Nuclear Information System (INIS) representatives from the following source:

Office of Scientific and Technical Information
P.O. Box 62
Oak Ridge, TN 37831
Telephone: 865-576-8401
Fax: 865-576-5728
E-mail: reports@adonis.osti.gov
Web site: http://www.osti.gov/contact.html

This report was prepared as an account of work sponsored by an agency of the United States Government. Neither the United States government nor any agency thereof, nor any of their employees, makes any warranty, express or implied, or assumes any legal liability or responsibility for the accuracy, completeness, or usefulness of any information, apparatus, product, or process disclosed, or represents that its use would not infringe privately owned rights. Reference herein to any specific commercial product, process, or service by trade name, trademark, manufacturer, or otherwise, does not necessarily constitute or imply its endorsement, recommendation, or favoring by the United States Government or any agency thereof. The views and opinions of authors expressed herein do not necessarily state or reflect those of the United States Government or any agency thereof.

ORNL/TM-2003/217

DETERMINATION OF THE APPLICABILITY OF HYDROSTATIC PROOF TESTING FOR DEMONSTRATING INTEGRITY OF HFIR PRIMARY-SYSTEM PIPING, VESSEL, AND RELATED COMPONENTS

R. D. Cheverton
Delta-21 Resources, Inc.
Oak Ridge, Tennessee 37830

J. R. Inger
Oak Ridge National Laboratory
Oak Ridge, Tennessee 37831-6369

Date Published: December 2003

Prepared by
OAK RIDGE NATIONAL LABORATORY
P.O. Box 2008
Oak Ridge, Tennessee 37831-6285
managed by
UT-Battelle, LLC
for the
U.S. DEPARTMENT OF ENERGY
under contract DE-AC05-00OR22725

CONTENTS

ACKNOWLEDGMENTS iii

ABSTRACT iv

1. INTRODUCTION 1

2. CRITERIA 3

3. TYPE, SIZE, AND LOCATION OF INITIAL FLAWS 6

4. BASIC LOADING CONDITIONS 7

5. STRESSES 8
   5.1 STRESSES CONSIDERED 8
   5.2 STRESS EQUATIONS 9

6. WELDS REQUIRING DETAILED ANALYSIS 13

7. IDENTIFICATION OF WELDS 14

8. CALCULATIONS 15

9. SUMMARY OF RESULTS AND CONCLUSIONS 16

REFERENCES 17

APPENDIX A: CALCULATION OF, σ(HT), $\sigma(E/F)$, AND $\sigma(S)$ FOR HFIR PRIMARY-SYSTEM 3-IN. AND LARGER PIPE AND COMPONENTS 34

ACKNOWLEDGMENTS

The authors wish to acknowledge contributions made by S. J. Chang and S. K. Iskander (review of report), P. C. Hambaugh and C. E. Dinkins (graphics), and Mary Wells (preparation of manuscript).

ABSTRACT

The integrity of the HFIR pressure vessel is demonstrated by periodic hydrostatic proof testing. Other components and piping in the primary system are, of course, subjected to the same pressure during testing of the vessel. This introduced the possibility of substituting hydrostatic proof testing for the usual ASME-specified inservice inspection (ISI) volumetric and penetrant testing of the piping and component welds. Because of constrained-thermal-expansion and seismic loads, however, not all piping welds are adequately tested by the vessel hydrostatic proof-test pressure, and higher pressures are not appropriate for the vessel. Using results of HFIR detailed piping analyses, each weld in the system was analyzed to determine which welds would be adequately tested during the vessel hydrostatic proof test. The results indicate that of the 3-in. and larger piping, 118 of the 167 circumferential welds and all of the axial welds are adequately tested. Also, all welds in the components are adequately tested. All other welds will be appropriately examined in accordance with the HFIR ISI program.

1. INTRODUCTION

Periodic hydrostatic proof testing is used to demonstrate the integrity of the HFIR pressure vessel[1,2], and the primary-system piping and related components (pumps, valves, heat exchangers, etc.) are exposed to the same hydro-test pressure. This introduces the possibility of substituting hydro testing for volumetric and surface inservice inspection (ISI) for demonstrating primary-system structural integrity. The ASME Code requires volumetric and surface (V/S) ISI for nuclear power plants[3], but for HFIR a hydro test has the potential for being much more reliable. Because of this higher reliability and also because of lower costs associated with hydro testing, it was suggested that ISI (V/S) of the pressure vessel and primary-system piping and components was not necessary[4,5]. For this to be acceptable, however, it is necessary that the potential for failure be greater during the hydro test than during worst-case operating conditions. The hydro-test conditions were selected accordingly, based on conditions associated with the highly irradiated portion (beltline region) of the vessel[1,2]. A later evaluation was performed for the piping[6]. At the time this latter evaluation was performed, the results of the HFIR piping flexibility analysis were not available, and thus "typical" secondary stresses that do not exist during the hydro test were used in the evaluation[7]. More recently, the original[8,9] and updated[10,11,12] flexibility-analysis reports were made available. The results of these studies indicated the need for another updated piping flexibility analysis, and this analysis was performed in November 1997[13]. Using this information, an updated evaluation of the applicability of hydro testing for the piping system, vessel, and components was performed[14] and was used as a basis for the ISI that was performed in conjunction with the March 12, 1998, hydrostatic proof test. Shortly thereafter, it was discovered that the piping-flexibility-analysis model included some incorrect spring loads and excluded three existing supports, all in the north/south pipe tunnel. These errors were corrected, and an updated analysis was performed[15]. Further examination of the model indicated that the snubber on the section of 20-in. pipe in the east/west tunnel was located incorrectly. This error was corrected, and a "final" updated piping analysis was performed[16] and used as input to another updated evaluation of the extent to which hydro testing could be substituted for ISI (V/S)[17]. The results indicated that hydro testing is adequate for the pressure vessel and components, most of the non-flux-type welds in the 4in. and larger piping and some of the welds in the smaller piping, which contains only non-flux-type welds, and some of the flux-type welds in the 4-in. and larger piping. The results also indicated that fewer welds than mentioned in Ref. 14 needed to be included for V/S in the ISI plan, and thus the ISI performed on March 12, 1998, was adequate.

In November 1998, an additional upgrade to the piping-flexibility-analysis model was made that consisted of (1) a small change in the normal operating temperature for some of the piping between the vessel outlet and the heat exchanger inlet and (2) an increase in the thermal coefficient of expansion for the circulating pumps. These changes affected only the constrained-thermal-expansion portion of the piping analysis, and the corresponding results were published in January 1999[18].

In August 2001, the portion of the 3-in. pressurizer line that runs from the 3-in.-line check valve to the primary-system 20-in. inlet line was added to the piping-flexibility-analysis model. It was expected that this relatively small line would have little effect on the rest of the system and, thus, was effectively calculated separately[19].

The piping analyses performed in Refs. 13, 15, 16, 18, and 19 provided, among other things, piping forces and moments for gravity, constrained-thermal-expansion, and seismic loads. The most recent and up-to-date data sets at the time of this writing are dated as follows: April 5, 1998 (gravity); April 20, 1998 (seismic), November 19, 1998 (thermal); and August 10, 2001 (gravity, constrained thermal expansion, and seismic for the 3-in. line).

The April 20, 1998, seismic data and the constrained-thermal-expansion data from Ref. 16 were used in Ref. 17, which did not address the 3-in. pipe. The April 20, 1998, seismic data, the November 19, 1998, constrained-thermal-expansion data, and the 3-in-pipe data[19] were used in the present report, which constitutes an update of Ref. 17. The results indicate that the hydro test adequately challenges all of the 3-in. welds and three more of the welds included in Ref. 17. With these exceptions, all of the welds adequately challenged by the hydro test are the same as those in Ref. 17.

Reference 17 includes an evaluation of primary-system piping with pipe sizes less than 3 in. (rabbit-facility, reactor-vent, vacuum-break, and gland-seal lines). This evaluation is not included in the present report but will be published in a separate document. Therefore, all of the smaller piping (< 3 in.) remains a part of the ASME Code-type ISI program.

2. CRITERIA

The failure mechanism of concern is propagation of flaws (sharp, crack-like defects). For the carbon steel components, the potential for propagation can be expressed as[20]

$$Potential = \frac{K_I}{K_c}, \tag{1}$$

where

$$\begin{aligned} K_I &= C\,\sigma\sqrt{\pi a} \\ &= \textit{stress intensity factor} \\ C &= \textit{factor depending on type flaw and structure} \\ \sigma &= \textit{far-field stress} \\ a &= \textit{flaw dimension} \\ K_c &= \textit{fracture toughness of material (critical value of } K_I\textit{)} \end{aligned} \tag{2}$$

For the hydro test to be adequate,

$$\frac{K_I(HT)}{K_c(HT)} \geq \frac{K_I(WC)}{K_c(WC)}, \tag{3}$$

where *WC* indicates the appropriate worst-case loading condition, and *HT* indicates the hydro-test condition.

The fracture toughness, K_c, which tends to decrease with decreasing temperature, is not sensitive to the small difference in hydro-test and minimum operating temperatures (85 compared to 80°F). Thus, it can be assumed that

$$K_c(HT) = K_c(WC). \tag{4}$$

Hydro tests are conducted periodically, and during the time between tests, flaw growth tends to take place due to fatigue and corrosion, increasing K_I. Taking this and Eq. (4) into account, Eq. (3) becomes

$$K_I(HT)_t \geq K_i(WC)_{t+\Delta t}, \tag{5}$$

where t = time of a hydro test
Δt = time between hydro tests

Using Eq. (2), assuming the values of C for membrane and bending stresses to be nearly the same, which is the case for the type flaws considered, and letting the flaw dimensions at time $t+\Delta t$ be $a+\Delta a$, Eq. (5) becomes

$$\frac{\sigma(HT)}{\sigma(WC)} \geq \left(1+\frac{\Delta a}{a}\right)^{1/2}, \tag{6}$$

where

Δa = flaw growth during the time between hydro tests.

Flaw growth for the flaws described below was calculated in a separate study[21] and was found to be very small (~ 3 $\times 10^{-3}$ in.).* Thus, Eq. (6) can be reduced to

$$\sigma(HT) \geq \sigma(WC) \tag{7}$$

Equation (7) cannot be applied to the belt-line region of the vessel because radiation reduces K_c during the time between hydro tests. Because of this reduction in K_c, the belt-line region of the vessel has the greatest potential for propagation of flaws. Thus, the hydro-test conditions (pressure, temperature, and frequency) were calculated on the basis of satisfying Eq. (3) for the belt-line region of the vessel[1,2]. No further treatment of the beltline is required nor included in this report. Other portions of the vessel, however, are included.

For the relatively ductile austenitic stainless steel piping and components and their associated non-flux-type welds, a more appropriate means of evaluating failure is the limit-load method. This method is included in Appendix C of Ref. 3 and is discussed in greater detail in Ref. 23. It is also applied to a leak-before-break evaluation in Ref. 7. In this latter reference, the relationship between the membrane stress (σ_m), critical bending stress (σ_b', bending stress at failure), and the flaw size (a) for the circumferential flaw described in Fig. 1, is as follows:

$$\sigma_b'/\sigma_f = \frac{2}{\pi}(2\sin\beta - \sin\theta), \tag{8}$$

$$\beta = \frac{\pi}{2}\left[1 - \frac{\theta}{\pi} - \sigma_m/\sigma_f\right], \tag{9}$$

where β defines the shift in the neutral axis due to the presence of the circumferential flaw, σ_f is the flow stress, and θ defines the arc length of the flaw at the average radius $(\overline{R})$.

Using Eqs. (8) and (9) to calculate $(\sigma_b' + \sigma_m)/\sigma_f$ as a function of σ_m/σ_f and θ, demonstrates that for reasonable values of the latter two parameters ($\sigma_m/\sigma_f = 0.1 - 0.3$ and $\theta/\pi = 0.05 - 0.5$), $(\sigma_b' + \sigma_m)/\sigma_f$ increases slightly ($\leq 4\%$) with increasing σ_m/σ_f for $\theta/\pi < 0.2$ and decreases with increasing σ_m/σ_f for $\theta/\pi \geq 0.2$. An increasing value of $(\sigma_b' + \sigma_m)/\sigma_f$ with increasing σ_m/σ_f indicates that the hydro test, which tends to have a high value of σ_m/σ_b, is not as severe a challenge to piping integrity, for the same value of $(\sigma_b' +$

*In recent studies pertaining to HFIR piping integrity, high-cycle fatigue, which could result in excessive flaw growth within days, was addressed, and was declared incredible[22].

$\sigma_m)/\sigma_f$, as worst-case loading conditions, for which some sections of the pipe can have relatively low values of σ_m/σ_b. On the other hand, a decreasing value of $(\sigma_b' + \sigma_m)/\sigma_f$ indicates that the hydro test is a more severe challenge for the same value of $(\sigma_b' + \sigma_m)/\sigma_f$. In view of the large uncertainty factor that is included in the calculation of the stresses (see Sect. 5.2), the above 4% can be ignored and the following criterion applied for establishing the adequacy of hydro testing:

$$(\sigma_b + \sigma_m)(HT) \geq (\sigma_b + \sigma_m)(WC), \tag{10}$$

where (*HT*) refers to the hydro test, and (*WC*) refers to worst-case operating conditions.

It is of interest to note that Eq. (10) is the same as Eq. (7). However, as discussed in Ref. 23 and implied in Ref. 3, it is not necessary to include displacement-limited loads, such as the constrained-thermal-expansion loads, in calculating σ_b and σ_m in Eq. (10) because a fully plastic condition precedes failure, and this precludes a significant contribution from displacement-limited loads.

The effect of flaw growth on $(\sigma_b' + \sigma_m)/\sigma_f$ was deduced from the parametric study mentioned above. The result was

$$\frac{\Delta(\sigma_b' + \sigma_m)\sigma_f}{\Delta(\theta/\pi)} \leq 3.0 \tag{11}$$

The maximum value of $\Delta(\theta/\pi)$ found in Ref. 21 for the 3-y period between hydro tests was 2×10^{-4}. Thus, the corresponding increase in $(\sigma_b' + \sigma_m)/\sigma_f$ due to crack growth is negligible, in which case Eq. (10) is adequate for evaluating the adequacy of hydro testing for the austenitic stainless steel piping and components and associated non-flux-type welds.

For axially oriented flaws (Fig. 2), the only stress is the hoop stress (σ_h), and thus the criterion is

$$\sigma_h(HT) \geq \sigma_h(WC) \tag{12}$$

The ductility of flux-type welds in austenitic stainless steel is sufficiently less than that of non-flux-type welds that failure can occur by ductile tearing prior to fully-plastic (limit-load) behavior. Thus, elastic-plastic fracture mechanics is used to evaluate the potential for failure of flux-type welds. Studies described in Ref. 23 indicate that the failure load for flux-type welds is less than that for non-flux-type welds and can be estimated by multiplying the limit-load critical value of $(\sigma_b + \sigma_m)$ by a factor. This implies that failure in the elastic-plastic regime is also controlled by $(\sigma_b + \sigma_m)$, and thus Eq. (10) applies for the flux-type welds in austenitic stainless steel as well as the non-flux type and also for carbon steel welds.

Reference 23 also states that there is not sufficient plasticity prior to failure of flux-type welds to prevent displacement-limited loads from contributing to failure. Thus, the constrained-thermal-expansion stresses must be included in Eq. (10) for flux-type welds.

3. TYPE, SIZE, AND LOCATION OF INITIAL FLAWS

The greatest potential for flaw growth exists for flaws perpendicular to the maximum principal stresses. Thus, axial and circumferential flaws normal to the surface are the ones of interest. The entire primary-system pressure boundary is exposed to the hydro-test pressure, and the impact of flaws in all areas of the pressure boundary was considered. The specific areas that tend to have unique features are the piping base material and axial and circumferential welds; components (heat exchangers, pumps, and valves); the vessel, other than its belt-line region; and bimetallic welds in the piping, vessel and components. As will be explained later, a preliminary qualitative analysis indicated that only the piping and only circumferential flaws in the piping needed to be considered in detail in this study.

For a flaw of reasonable length in the pipe to be critical, it must extend through the wall (Figs. 1 and 2)[6]. The greater the initial length of these flaws, the greater the potential for propagation by static loading to failure and by fatigue. A length large compared to the calculated growth over the life of the system and also a flaw-length that would result in a reasonable chance of flaw detection by leak checking was considered reasonable. On the basis of previous related studies[6], a length of 3 in. was selected for the 3-in. and larger pipe.

Equations (7) and (10) indicate that the characterization of the assumed flaw is not important. This is not the case, however, because the calculated value of $\Delta a/a$ is dependent on flaw characteristics, and, as will be demonstrated later, so is the far-field stress. In the course of this study, it was determined that the effect of flaw size on the far-field stress was small.

4. BASIC LOADING CONDITIONS

Equation (3) indicates that there are two basic loading conditions that must be considered: (1) hydro test and (2) worst-case operation. Two worst-case operating conditions exist: (1) emergency/faulted (*E/F*) and (2) seismic. The *E/F* condition consists of (1) the primary-system pressure reaching the rupture-disc value and (2) a vessel temperature as low as 80°F. It is assumed that the *E/F* and seismic events do not occur simultaneously because the frequencies of occurrence of both are very small ($4 \times 10^{-5} y^{-1}$ for the *E/F* event and $5 \times 10^{-4} y^{-1}$ for the design-basis seismic event)[24,25] and their durations are short.

Additional loads that must be considered are dead weight (gravity), constrained thermal expansion, and water hammer. Gravity loads are the same for the basic load cases and thus drop out of Eqs. (7) and (10). Constrained-thermal-expansion loads are essentially zero at room temperature and thus do not exist during the hydro test but do exist during worst-case operation, which is most likely to take place at elevated temperatures (normal operating temperatures). Water hammer is not likely to take place during either of the worst-case events because of their small frequencies, and because there appears to be no credible way of producing a significant water-hammer event in the HFIR primary system[26]. Thus, water-hammer loads are not considered.

As explained in Sect. 2, depending on the type material a flaw is assumed to reside in, it may or may not be necessary to include the constrained-thermal-expansion loads in the worst-case loading conditions.

In summary, then, there are three basic loading conditions that must be considered: (1) hydro test, which does not include constrained-thermal-expansion loads; (2) *E/F*, which may or may not include constrained-thermal-expansion loads and does not include seismic loads; and (3) seismic, which is assumed to occur during normal operation and may or may not include constrained-thermal-expansion loads.

5. STRESSES

5.1 STRESSES CONSIDERED

In addition to stresses resulting from the loads defined in Sect 4, there are residual stresses and stresses associated with bimetallic welds. Residual stresses are the same for the three basic loading conditions and thus drop out of Eqs. (7) and (10).

Bimetallic welds, which exist at the heat exchanger head-to-tube-sheet juncture, the vessel lower-extension attachment to the vessel hemispherical head, and the vessel inlet-nozzle pipe attachment, introduce differential thermal-expansion stresses that are system-temperature dependent. As discussed in Ref. 21, the axial differential-expansion stresses in the bimetallic welds are a maximum at room temperature and thus decrease as the system warms up to "operating" temperature. The minimum temperature associated with the *WC* condition is essentially the same as or higher than that for the hydro test. Thus, as a conservative measure, the axial differential expansion stress can also be left out of Eqs. (7) and (10).

The circumferential stress induced by differential expansion in bimetallic welds is also a "maximum" at room temperature. The maximum occurs at the juncture of the two materials and is positive in the stainless steel portion and negative in the carbon steel portion. The stress approaches zero in a short distance from the juncture and thus has little effect on axial extension of an axially oriented through-the-wall flaw. During warm-up, the positive hoop stress in the stainless steel decreases, and the negative stress in the carbon steel becomes less negative but remains negative at the *WC* loading condition temperatures. Thus, it is conservative to ignore the warm-up stresses. Eliminating these stresses in the bimetallic welds leaves only the pressure-induced stresses for the circumferential direction. Because the pressure stresses are higher for the hydro test than for the *WC* conditions, Eqs. 7 and 10 are satisfied for hoop stresses, and thus only circumferential flaws and axial stresses need to be considered in detail. The stress at room temperature (cool-down stress) is the same for both the hydro test and *WC* conditions and thus cancels out of Eqs. (7) and (10).

At the juncture of the heat-exchanger hemispherical head and tube sheet, there is a structural discontinuity that results in pressure-induced bending stresses [$\sigma_b(d)$]. The equation for $\sigma_b(d)$ is derived in Ref. 21 and is included in this study. However, because the hydro-test pressure is greater than the *WC* pressures, values of $\sigma_b(d)$ are always higher for the hydro test.

Constrained-thermal-expansion and seismic loads are applied to the vessel and components at the pipe attachments only. Because the section moduli of welds in the vessel, heat exchangers and pumps, with the exception of the pipe-attachment (pipe-to-component) welds, are very large compared to those for welds in the pipe, stresses in the vessel (including the vessel's lower extension bimetallic weld), heat exchanger, and pump welds due to constrained-thermal-expansion and seismic loads are very small compared to the pressure stresses. Based on the above arguments, it is concluded that Eqs. (7) and (10) are satisfied for the *E/F* and seismic conditions for the three "components" mentioned, with the possible exception of the pipe attachment welds, which are evaluated as piping, and for all axial flaws in the piping. Thus, only axial stresses in the piping must be considered in detail.

For this latest revision of the report, the attachment welds for the vessel's 16-in. inlet lines are taken as the bimetallic welds at the junctures of the main inlet nozzles and the transition sections between the nozzles and the 16-in. pipe (nodes 696 and 705; Table 1 and Fig. 3), and the transition sections (elements 242 and 249) were considered to be the same 16-in. pipe used elsewhere in the primary

system. This later consideration was also included in Ref. 17, and is conservative because the actual transition section has a larger section modulus. The specified location of the vessel/piping attachment weld in Ref. 17 was the nozzle weld in the vessel. This was excessively conservative because of the relatively large size of that weld (32 in. diameter and extending through the 3-in. vessel wall) compared to the 16-in. pipe (16.-in. OD and 0.5-in. wall). As indicated above, moving the specified attachment location from the vessel wall to the nozzle/transition-section juncture is still somewhat conservative.

As mentioned in Sect. 3 and explained above, the flaw of primary concern is a circumferential through flaw (Fig. 1). The presence of a circumferential flaw shifts the neutral axis of the cross section and results in an axial bending moment if axial forces are present. The shift in the neutral axis was calculated in Ref. 21 for each pipe size.

Constrained-thermal-expansion, seismic- and gravity-induced axial forces and bending moments for most of the HFIR primary-system piping and components were calculated in Refs. 8 and 9 at the time of the HFIR design effort and later (1988) in Ref. 10 during a reevaluation of the structural integrity of the HFIR pressure vessel. At this latter time, the calculations were performed using the GEMINI computer code[27], and the "same" code was initially used for the present study. Preliminary results indicated that the most recent version of the GEMINI code contained errors. Because of this and an apparent lack of documented quality assurance for GEMINI, the final analysis for the Ref. 17 study was performed with ANSYS[28], which is a well-established structural code that has proper documentation of appropriate quality assurance. The results agreed well with the results obtained in 1988 with the GEMINI code[10], indicating that those earlier GEMINI results were reasonably accurate.

The first set of ANSYS results were used as input to the Ref. 14 evaluation of the applicability of hydro testing for demonstrating the integrity of the piping and components. Soon thereafter, it was discovered that the ANSYS model for HFIR included some incorrect spring-hanger preloads and also excluded three existing vertical supports, all in the north/south tunnel. These errors were corrected, and an updated analysis was performed[15]. Further examination of the ANSYS HFIR model indicated that the snubber on the section of 20-in. pipe located in the east/west tunnel was 30 in. west of its actual location. This error was corrected, and another updated piping analysis was performed for seismic loading[16]. Seismic-induced axial loads and moments from this latter analysis (ANSYS output dated April 20, 1998) and constrained-thermal-expansion-induced axial loads and moments from the Ref. 15 analysis (snubbers have no effect on static loads) (ANSYS output dated April 7, 1998) were used for the hydro-test-applicability evaluation in Ref. 17. Since then, the normal operating temperature for piping between the outlet of the vessel and inlet to the heat exchangers was increased slightly, and the coefficient of thermal expansion of the pump housing was increased. The changes affected the constrained-thermal-expansion analysis only. The corresponding constrained-thermal-expansion forces and moments are included in Ref. 18 and were used in the present report, which constitutes a revision to Ref. 17.

Also included in the present report is the 3-in. pressurizer line. The forces and moments for this line are included in Ref. 19.

5.2 Stress equations

Equations for the stresses that must be considered are as follows:

Pressure-induced axial membrane stress [$\sigma_m(p)$]:

$$\sigma_m(p) = \frac{p}{2}\left(\frac{\overline{R}}{t}\right) \tag{13}$$

Pressure-induced axial bending stress [$\sigma_b(p)$]:

$$\sigma_b(p) = \sigma_b(A,p) + \sigma_b(d) = \frac{p\pi D_i^2 h}{4Z} + \frac{p}{2}\left(\frac{\overline{R}}{t}\right)\left[\frac{3(1-\nu)}{(1+\nu)}\right]^{1/2} \tag{14}$$

Pressure-induced hoop stress [σ_{hoop} (p)]:

$$\sigma_{hoop} = p\left(\frac{\overline{R}}{t}\right) \tag{15}$$

Constrained-thermal-expansion and seismic-induced axial bending stresses:

$$\sigma_b(e) = \frac{1}{Z}\left[\left(M_e(y)\right)^2 + \left(M_e(z)\right)^2\right]^{1/2} + \frac{F_e h}{Z} \tag{16}$$

$$\sigma_b(s) = \frac{1}{Z}\left[\left(M_s(y)\right)^2 + \left(M_s(z)\right)^2\right]^{1/2} + \frac{F_s h}{Z} \tag{17}$$

Contrained-thermal-expansion and seismic-induced axial membrane stresses

$$\sigma_m(e) = \frac{4F_e}{\pi\left(D_o^2 - D_i^2\right)} \tag{18}$$

$$\sigma_m(s) = \frac{4F_s}{\pi\left(D_o^2 - D_i^2\right)} \tag{19}$$

where

$\sigma_b(e)$	=	axial bending stress due to constrained thermal expansion
$\sigma_b(s)$	=	axial bending stress due to seismic loading
$\sigma_b(p)$	=	axial bending stress due to pressure
$\sigma_m(e)$	=	axial membrane stress due to constrained thermal expansion
$\sigma_m(s)$	=	axial membrane stress due to seismic loading
$\sigma_m(p)$	=	axial membrane stress due to pressure

$\sigma_b(A,p)$	=	axial bending stress due to pressure-induced axial load
$\sigma_b(d)$	=	axial bending stress due to pressure as a result of structural discontinuity
$\sigma(HT)$	=	"total" axial stress for hydro-static loading
$\sigma(E/F)$	=	"total" axial stress for emergency/faulted condition
$\sigma(S)$	=	"total" axial stress for normal operation and seismic loading
F_e	=	axial force due to constrained thermal expansion
F_s	=	axial force due to seismic loading
$M_e(y)$	=	axial moment, about y axis, due to constrained thermal expansion
$M_e(z)$	=	axial moment, about z axis, due to constrained thermal expansion
$M_s(y)$	=	axial moment, about y axis, due to seismic loading
$M_s(z)$	=	axial moment, about z axis, due to seismic loading
h	=	shift in neutral axis due to presence of circumferential, through-wall flaw
D_i	=	inside diameter of pipe
D_o	=	outside diameter of pipe
$\bar{R}$	=	mean radius of pipe
t	=	pipe wall thickness
ν	=	Poisson's ratio
E	=	modulus of elasticity
Z	=	section modulus
p	=	pressure
$p(HT)$	=	hydro-test pressure
$p(E/F)$	=	emergency/faulted-condition pressure
$p(\mathrm{N})$	=	normal operating pressure

Combining the appropriate axial stresses, and ignoring the differential expansion term for the nonbimetallic welds, yields

$$\begin{aligned}\sigma(HT) &= \sigma_m(p) + \sigma_b(p) \\ &= \frac{p(HT)}{2}\left(\frac{\bar{R}}{t}\right) + \frac{p(HT)\pi D_i^2 h}{4Z} + \frac{p(HT)}{2}\left(\frac{\bar{R}}{t}\right)\left[\frac{3(1-\nu)}{(1+\nu)}\right]^{1/2}\end{aligned} \tag{20}$$

$$\begin{aligned}\sigma(E/F) &= \sigma_m(p) + \sigma_b(p) + \sigma_b(e) + \sigma_m(e) \\ &= \frac{p(E/F)}{2}\left(\frac{\bar{R}}{t}\right) + \frac{p(E/F)\pi D_i^2 h}{4Z} + \frac{p(E/F)}{2}\left(\frac{\bar{R}}{t}\right)\left[\frac{3(1-\nu)}{(1+\nu)}\right]^{1/2} \\ &\quad + 1.8\left\{\frac{1}{Z}\left[\left(M_e(y)\right)^2 + \left(M_e(z)\right)^2\right]^{1/2} + \frac{F_e h}{Z} + \frac{4F_e}{\pi\left(D_o^2 - D_i^2\right)}\right\}\end{aligned} \tag{21}$$

$$
\begin{aligned}
\sigma(S) &= \sigma_m(p) + \sigma_b(p) + \sigma_b(s) + \sigma_m(s) \\
&= \frac{p(N)}{2}\left(\frac{\bar{R}}{t}\right) + \frac{p(N)\pi D_i^2 h}{4Z} + \frac{p(N)}{2}\left(\frac{\bar{R}}{t}\right)\left[\frac{3(1-\nu)}{(1+\nu)}\right]^{1/2} \\
&+ 1.8\left\{\frac{1}{Z}\left[\left(|M_e(Y)| + M_s(y)\right)^2 + \left(|M_e(Z)| + M_s(Z)\right)^2\right]^{1/2} + \frac{(F_e + F_s)h}{Z} + \frac{4(F_e + F_s)}{\pi\left(D_o^2 - D_i^2\right)}\right\}
\end{aligned}
\tag{22}
$$

The uncertainty in stresses due to constrained-thermal-expansion- and seismic-induced bending and axial loads is large compared to that for pressure-induced stresses. The ratio of uncertainty factors is assumed to be 1.8 and is applied to the last three terms in Eqs. (21) and (22).

Absolute values of M_e are used in Eq. (22) because M_s oscillates, resulting in positive values of bending stress on the same side of the pipe at the same time. By contrast, bending due to $F_e x\, h$ always produces a negative stress on the side of the pipe containing the flaw, when F_e is negative, and thus the calculated sign of F_e is retained.

The third term in Eqs. (20), (21), and (22) applies only to the weld joining the heat exchanger head to the tube sheet. As indicated in Sect. 6, it is not necessary to evaluate this weld, and thus these terms are not used in this evaluation.

6. WELDS REQUIRING DETAILED ANALYSIS

All welds for which hydro testing is to be substituted for ISI must satisfy either Eq. (3) (those in the vessel beltline region) and Eq. (7), or Eq. (10). Based on the information in Sects. 1, 3, and 5, it is apparent that only the piping and only postulated circumferential flaws in circumferential welds of the piping need to be evaluated in detail in this study.

The extent of the piping analysis is dependent on whether the weld is a flux type (submerged arc or coated rod) or non-flux type (tungston inert gas arc weld). As discussed in Sect. 2, non-flux-type welds in austenitic stainless steel pipe are sufficiently ductile that displacement-limited loads (i.e., constrained-thermal-expansion loads) do not contribute significantly to failure of the pipe (a flaw will not propagate before plastic collapse of the pipe). Thus, $\sigma(E/F)$ and $\sigma(S)$ need not include constrained-thermal-expansion stresses for non-flux-type welds.

All of the HFIR primary-system 4-in. and smaller pipe circumferential welds and the attachment welds for all weldolets, sweepolets, and branch-connection weld-neck flanges are of the non-flux type. Each of the welds in the 3-in. and larger pipe are identified accordingly in Sect. 7. Welds in the beltline region of the vessel were initially evaluated in Refs. 1 and 2 and most recently in Refs. 29 and 30.

The specific piping and corresponding welds considered in this report are indicated in Figs. 3 and 4 and Table 1. As indicated, the pipe sizes range from 3-in. to 20-in. A preliminary version of this report[17] also addressed pipe sizes less than 3-in., which occur in the rabbit-facility vacuum-break, gland-seal and reactor vent lines. An updated evaluation of these lines will be included in a separate report.

7. IDENTIFICATION OF WELDS

All of the HFIR primary-system circumferential welds in the 3-in and larger piping are identified in Table 1 and Figs. 3 and 4. Table 1 also indicates whether a weld is a flux type or non-flux type and includes the three-dimensional spatial coordinates of the pipe/weld centerline relative to an arbitrary origin. This information was obtained from Refs. 10–13, 19, and 31–33. In addition, weld-inspection records were examined to verify the type of weld (flux or non-flux). It was determined that welds made off-site by the pipe-subassembly fabricator are flux type (with few exceptions), and welds made at the site as either shop or field welds are non-flux type.

8. CALCULATIONS

Calculations of $\sigma(HT)$, $\sigma(E/F)$ and $\sigma(S)$, and a comparison of the results with the criterion described by Eq. (10) are included in Appendix A for the 3-in. and larger pipe. A summary of results is included in the following section (Sect. 9).

9. SUMMARY OF RESULTS AND CONCLUSIONS

The results of this study indicate that hydrostatic proof testing is a satisfactory method of demonstrating the structural integrity of 71 of the 85 non-flux circumferential welds, 47 of the 82 flux-type circumferential welds, and all of the axial welds in the HFIR primary-system 3-in. and larger piping. It is also satisfactory for all welds in the primary-system pressure vessel, heat exchangers, pumps, and valves. Specific welds in the 4-in. and larger pipe that must be subjected to ISI (V/S) are identified in Table 2.

In the above analyses, growth of hypothetical flaws during the time between hydro tests was considered and was found to be negligible.

REFERENCES

1. R. D. Cheverton, J. G. Merkle, and R. K. Nanstad, *Evaluation of HFIR Pressure-Vessel Integrity Considering Radiation Embrittlement*, ORNL/TM-10444, Oak Ridge National Laboratory, April 1988.

2. R. D. Cheverton and R. K. Nanstad, *Evaluation of HFIR Vessel Surveillance Data and Hydro-Test Conditions*, ORNL/TM-12758, Oak Ridge National Laboratory, August 5, 1994.

3. ASME Boiler and Pressure Vessel Code, Section XI, Division 1.

4. R. D. Cheverton, *Substitution of Hydro Testing for Volumetric Inspection of the HFIR Vessel Welds*, Letter to J. R. Inger, Oak Ridge National Lab., January 5, 1996.

5. R. D. Cheverton, *Substitution of Hydro Testing for Volumetric Inspection of the HFIR Primary Piping*, Letter to J. R. Inger, Oak Ridge National Lab., January 10, 1996.

6. R. D. Cheverton, *Leak-Before-Break Analysis for HFIR Primary-System Piping*, RDC/LTR-96-1, October 11, 1996, attachment to letter from R. D. Cheverton to J. R. Inger, Oak Ridge National Lab., October 11, 1996.

7. R. L. Sindelar, G. F. Mertz, and K. J. Stoner, *Reactor Materials Program Leak-Before-Break Analyses of Reactor Process Water System Piping (U)*, Task Number 89-036-1, Savannah River Lab., WSRC-RP-90-91, March 1, 1990.

8. *Piping Flexibility Analysis, Primary Coolant Loop, Reactor Inlet Line*, SMB-1011, Service Bureau Corporation, June 28, 1961.

9. *Piping Flexibility Analysis, Primary Coolant Loop, Reactor Outlet Line*, SMB-1001, Service Bureau Corporation, June 27, 1961.

10. Seismic Evaluation of the ORNL High Flux Isotope Reactor, Calculation 87257.01-C-003, EQE Engineering, March 29, 1988.

11. Seismic Evaluation of the ORNL High Flux Isotope Reactor, Calculations 87257.01-C-28, 29, and 30, EQE Engineering, May 1989.

12. Seismic Evaluation of the ORNL High Flux Isotope Reactor, Calculation 87257.01-C-31, EQE Engineering, February 1989.

13. HFIR Primary Coolant Piping Reanalysis with ANSYS Model, Calculation No. 52281.13-C-02, EQE Engineering, November 1997.

14. R. D. Cheverton and J. R. Inger, *Determination of the Applicability of Hydrostatic Proof Testing for Demonstrating Integrity of HFIR Primary-System Piping, Vessel, and Related Components*, RDC/JRI/RRD/LTR-97-2, February 9, 1998.

15. HFIR Primary Coolant Piping Reanalysis with ANSYS Model, Calculation No. 52281.13-C-02, Revision 1, Attachment G, EQE Engineering, April 8, 1998.

16. HFIR Primary Coolant Piping Reanalysis with ANSYS Model, Calculation No. 52281.13-C-02, Revision 2, Attachment L, EQE Engineering, May 4, 1998.

17. R. D. Cheverton and J. R. Inger, *Determination of the Applicability of Hydrostatic Proof Testing for Demonstrating Integrity of HFIR Primary System Piping, Vessel, and Related Components*, RDC/JRI/RRD/LTR-97-2/R1, August 1998.

18. EQE Calculation No. 52281.13-C-02, Revision 4, January 28, 1999.

19. EQE Calculation No. 52281.13-C-03, Revision 0, August 16, 2001.

20. S. T. Rolfe and J. M. Barsom, *Fracture and Fracture Control in Structures, Applications of Fracture Mechanics*, 1977, Prentice-Hall, Inc.

21. R. D. Cheverton and J. R. Inger, *Growth of Hypothetical Flaws in the HFIR Primary-System Piping and Components During the Time Between Hydrostatic Proof Tests*, RDC/JRI/RRD/LTR-97-1, February 9, 1998.

22. R. D. Cheverton, *Probability of Failure of the HFIR Primary Piping*, RDC/ORNL/RRD/LTR-01-1, September 2001.

23. Evaluation of Flaws in Austenitic Steel Piping, EPRI-NP-4690-SR, April 11, 1986.

24. R. D. Cheverton, *An Evaluation of Life Extension of the HFIR Pressure Vessel*, ORNL/TM-12877, Oak Ridge National Laboratory, December 1994.

25. D. W. Coats and R. C. Murray, *Natural Phenomena Hazards Modeling Project: Seismic Hazard Levels for the Department of Energy Sites*, UCRC-53582, Rev. 1, Lawrence Livermore National Laboratory, November 1984.

26. Personal Communication with Mark Linn (ORNL/RRD), 1997.

27. "GEMINI — A Computer Program for Two- and Three-Dimensional Static and Seismic Structural Analysis," Lawrence Livermore National Laboratory, October 1984.

28. "ANSYS Program Version 5.3 User's Manual," ANSYS, Inc., July 10, 1996.

29. R. D. Cheverton and T. L. Dickson, *HFIR Vessel Life Extension with Enlarged HB-2 and HB-4 Beam Tubes*, ORNL/TM-13698, December 1998.

30. R. D. Cheverton and J. W. Bryson, *HFIR Vessel Pressure/Temperature Limits Corresponding to the Upgrade Design*, ORNL/TM-1999/181/R1, March 2000.

31. Southwest Fabricating and Welding Co., Inc., Power Division, Drawing 75X-84314-1, 10/31/62, HFIR Piping-System Outlet Piping.

32. Southwest Fabricating and Welding Co., Inc., Power Division, Drawing 75X-84314-2, 10/31/62, HFIR Primary-System Inlet Piping.

33. H. K. Ferguson Co., High Flux Isotope Reactor (95-1) H.P. Primary Coolant Piping Installation Data and Weld Record (Drawing), January 10, 1964.

34. *Research Reactors Division Inservice Inspection and Testing Manual*, ORNL/RRD/INT-72, Rev. 3, in preparation.

Table 1. Identification of and spatial coordinates for HFIR primary-system large-pipe (3-in.-diameter and larger) circumferential welds

Pipe	I/O[a]	Descriptor[b]	Node[c]	Type[d]	Weld[e] No.	X[f] (in.)	Y[f] (in)	Z[f] (in.)
3-in.	I	PL	7652	NF	1054-W58	881	173	711
			7653	NF	1054-W57	885	177	710
			7654	NF	1054-W56	894	177	708
			7655	NF	1054-W55	898	173	708
			7657	NF	1054-W54	898	110	708
			7658	NF	1054-W53	898	105	703
4-in.	I	PR, Sweepolet	1030	NF	1056-W23	881	161	801
			1010	NF	1056-W22	873	169	801
			1011	NF	1056-W21	869	173	807
			1012	NF	1056-W20	869	173	843
			1014	NF	1056-W19	857	173	843
			1015	NF	1056-W18	857	173	807
			1016	NF	1056-W17	851	173	801
			1017	NF	1056-W16	780	173	801
			1018	NF	1056-W15	774	179	801
			1020	NF	1056-W13	774	183	793
			1021	NF	1056-W14	774	183	805
10-in.	I	110	652	NF	1020-W1	881	161	754
			753	F	1020-W2	861	161	774
			754	F	1020-W3	857	161	784
			755	F	1020-W4	857	161	834
			756	NF	1020-W5	842	161	849
			757	NF	1020-W9	788	161	849
		(Pipe/GV)	758	NF	1020-W6	736	161	849
		(GV/CV)	761	NF	1020-W7	720	161	849

Table 1 (cont'd.)

Pipe	I/O[a]	Descriptor[b]	Node[c]	Type[d]	Weld[e] No.	X[f] (in.)	Y[f] (in)	Z[f] (in.)
10-in.	I	(CV/P)	762	NF	1020-W8	696	161	849
14-in.	I	110, (EL/P)	844	F	1176-W5	678	148	842
			828	NF	1176-W4	657	127	842
			827	NF	1176-W3	619	127	842
		Flange pair	826 826	NF F	1176-W2 1176-W1	604 604	127 127	836 836
	I	(F/HX)	825	NF	1176-W0	599	127	831
10-in.	I	111	655	NF	1011-W1	881	161	946
			764	F	1011-W2	861	161	966
			765	F	1011-W3	857	161	976
			766	F	1011-W4	857	161	1033
			767	NF	1011-W5	842	161	1048
		(Pipe/GV)	769	NF	1011-W6	736	161	1048
		(GV/CV)	772	NF	1011-W7	720	161	1048
		(CV/P)	773	NF	1011-W8	696	161	1048
14-in.	I	111, (EL/P)	843	F	1006-W5	678	148	1034
			832	NF	1006-W4	657	127	1034
			831	F	1006-W3	619	127	1034
		Flange pair	830 830	F F	1006-W2 1006-W1	604 604	127 127	1028 1028
		(F/HX)	829	F	1006-W0	599	127	1023
10-in.	I	112	658	NF	1010-W1	881	161	1138
			775	F	1010-W2	861	161	1158
			776	F	1010-W3	857	161	1168

Table 1 (cont'd.)

Pipe	I/O[a]	Descriptor[b]	Node[c]	Type[d]	Weld[e] No.	X[f] (in.)	Y[f] (in)	Z[f] (in.)
10-in.	I	112	777	F	1010-W4	857	161	1225
			778	NF	1010-W5	842	161	1240
		(Pipe/GV)	780	NF	1010-W6	736	161	1240
		(GV/CV)	783	NF	1010-W7	720	161	1240
		(CV/P)	784	NF	1010-W8	696	161	1240
14-in.	I	112, (EL/P)	842	F	1004-W5	678	148	1226
			836	NF	1004-W4	657	127	1226
			835	F	1004-W3	619	127	1226
		Flange pair	834 834	F F	1004-W2 1004-W1	604 604	127 127	1220 1220
		(F/HX)	833	F	1004-W0	599	127	1214
10-in.	I	113	660	F	1009-W1	881	161	1183
			1022	F	1009-W2	881	161	1212
			1023	F	1009-W3	881	161	1272
			1024	F	1009-W4	881	161	1331
			1025	F	1009-W5	881	161	1343
			663	F	1009-W6	881	161	1401
			664	F	1009-W7	877	161	1412
			665	F	1009-W8	861	161	1427
			666	NF	1009-W9	851	161	1432
		(Pipe/GV)	668	NF	1009-W10	736	161	1432
		(GV/CV)	671	NF	1009-W11	720	161	1432
10-in.	I	(CV/P)	672	NF	1009-W12	696	161	1432
14-in.	I	113, (EL/P)	841	F	1002-W5	678	148	1418
			840	NF	1002-W4	657	127	1418

Table 1 (cont'd.)

Pipe	I/O[a]	Descriptor[b]	Node[c]	Type[d]	Weld[e] No.	X[f] (in.)	Y[f] (in)	Z[f] (in.)
14-in.	I	113, (EL/P)	839	F	1002-W3	619	127	1418
		Flange pair	838 838	F F	1002-W2 1002-W1	604 604	127 127	1412 1412
		(F/HX)	837	NF	1002-W0	599	127	1407
16-in.	I	Main	696	F	CW-1/Ext	318	108	627
			697	NF	1008-W6	307	108	638
			699	F	1008-W5	307	108	661
			698	NF	1008-W4	318	108	666
			700	NF	1008-W3	380	108	666
			701	F	1008-W2	391	108	661
			705	F	CW-2/Ext.	402	108	543
			706	NF	1007-W18	413	108	532
			707	F	1007-W17	425	108	527
			708	NF	1007-W16	441	108	543
			709	NF	1007-W15	441	108	605
			710	F	1007-W14	436	108	616
20-in.	I	Main, Tee	712	F	1007-W13	421	108	627
			703	F	1008-W1	401	108	647
			713	NF	1007-W12	411	122	636
20-in.			714	F	1007-W21	411	148	636
			716	F	1007-W20	411	175	636
			717	F	1007-W19	426	158	636
			1028	NF	1007-W11	441	158	636
			720	F	1007-W1	567	158	636

Table 1 (cont'd.)

Pipe	I/O[a]	Descriptor[b]	Node[c]	Type[d]	Weld[e] No.	X[f] (in.)	Y[f] (in)	Z[f] (in.)
20-in.	I	Venturi	721	F	1007-W2	581	158	636
			722	F	1007-W3	617	158	636
			723	F	1007-W4	630	158	636
			724	NF	1007-W5	665	158	636
			649	NF	1007-W6	851	161	636
			650	F	1007-W7	881	161	666
			653	F	1007-W8	881	161	842
			656	NF	1007-W9	881	161	1034
			659	F	1007-W10	881	161	1167
10-in.	O	110	695	NF	1019-W1	827	124	650
			786	F	1019-W2	853	127	675
			787	NF	1019-W3	857	127	686
			788	F	1019-W4	857	127	746
			789	NF	1019-W5	842	127	761
			790	NF	1019-W11	788	127	761
			791	NF	1019-W6	758	127	761
			793	NF	1019-W7	727	127	761
			795	NF	1019-W8	631	127	761
14-in.	O	110	796	NF	1019-W9	619	127	761
		Flange pair	797 797	NF F	1019-W10 1019-W12	604 604	127 127	768 768
			798	NF	1019-W13	599	127	773
10-in.	O	111	732	NF	1005-W1	881	127	848
			799	F	1005-W2	861	127	868
			800	F	1005-W3	857	127	878
			801	F	1005-W4	857	127	938

Table 1 (cont'd.)

Pipe	I/O[a]	Descriptor[b]	Node[c]	Type[d]	Weld[e] No.	X[f] (in.)	Y[f] (in)	Z[f] (in.)
10-in.	O	111	802	NF	1005-W5	842	127	953
			804	NF	1005-W6	758	127	953
			806	NF	1005-W7	727	127	953
			808	F	1005-W8	632	127	953
14-in.	O	111	809	F	1005-W9	619	127	953
		Flange pair	810 810	F F	1005-W10 1005-W11	604 604	127 127	960 960
			811	F	1005-W12	599	127	965
10-in.	O	112	735	NF	1003-W1	881	127	1040
			812	F	1003-W2	861	127	1060
			813	NF	1003-W3	857	127	1070
			814	F	1003-W4	857	127	1131
			815	NF	1003-W5	842	127	1146
			817	NF	1003-W6	758	127	1146
			819	NF	1003-W7	727	127	1146
			821	F	1003-W8	632	127	1146
14-in.	O	112	822	F	1003-W9	619	127	1146
		Flange pair	823 823	F F	1003-W10 1003-W11	604 604	127 127	1152 1152
			824	F	1003-W12	599	127	1156
10-in.	O	113	737	NF	1001-W1	881	127	1086
			1029	F	1001-W2	881	127	1112
			739	F	1001-W3	881	127	1186
			742	F	1001-W4	881	127	1322
			743	NF	1001-W5	866	127	1337

Table 1 (cont'd.)

Pipe	I/O[a]	Descriptor[b]	Node[c]	Type[d]	Weld[e] No.	X[f] (in.)	Y[f] (in)	Z[f] (in.)
10-in.	O	113	745	NF	1001-W6	758	127	1337
			747	NF	1001-W7	727	127	1337
			749	F	1001-W8	632	127	1337
14-in.	O	113	750	F	1001-W9	619	127	1337
		Flange pair	751 751	F F	1001-W10 1001-W11	604 604	127 127	1344 1344
			752	NF	1001-W12	599	127	1349
18-in.	O	Main	680	F	1000-W11	378	-42	601
			681	NF	1000-W10	388	-42	611
			682	NF	1000-W9	410	-42	632
			683	F	1000-W8	430	-15	650
			685	NF	1000-W7	430	97	650
			687	NF	1000-W6	457	124	650
			691	F	1000-W1	639	124	650
			728	NF	1000-W2	854	127	650
			729	F	1000-W3	881	127	677
			732	F	1000-W4	881	127	860[g]
			736	F	1000-W5	881	127	1070

[a]Inlet (I) or outlet (O) piping as referred to in Refs. 8, 9, 31, 32, and 33.
"Inlet" piping extends from the heat exchanger discharge to the vessel inlet, while "outlet" piping extends from the vessel discharge to the heat exchanger inlet.

[b]Numbers 110, 111, 112, and 113 refer to portions of systems identified in Figs. 3 and 4 and Refs. 8 and 9.

Main: main or trunk line
Pipe/GV: pipe to gate-valve juncture
GV/CV: gate-valve to check-valve juncture
CV/P: check-valve to pump juncture
EL/P: elbow to pump juncture
F/HX: flange to heat-changer juncture
PR: pressure-relief system.
PL: pressurizer line

Table 1 (cont'd.)

[c]Node numbers used in Refs. 10, 13, 18, and 19.
[d]Flux-type (F) or non-flux-type (NF) welds.
[e]Weld numbers referred to in Ref. 34.
[f]*X, Y, Z*: spatial coordinates with reference to arbitrary origin (Refs. 10, 13, and 21).

[g]Actual location. ANSYS assumes $Z = 848$ in. (See weld no. 1005-W1).

Table 2. Circumferential welds in the 4-in. and larger pipe for which hydrostatic proof testing is not a satisfactory means of demonstrating structural integrity

Pipe	I/O	Descriptor	Node	Weld no.
4-in.	I	PR	1016	1056-W17
			1014	1056-W19
			1012	1056-W20
			1011	1056-W21
			1010	1056-W22
			1030	1056-W23
10-in.	I	110	652	1020-W1
			753	1020-W2
			754	1020-W3
		111	655	1011-W1
			764	1011-W2
			765	1011-W3
			767	1011-W5
		112	658	1010-W1
			775	1010-W2
			776	1010-W3
			777	1010-W4
			778	1010-W5
		113	663	1009-W6
			664	1009-W7
10-in.	I	113	665	1009-W8
14-in.	I	110	844	1176-W5
		111	829	1006-W0
			843	1006-W5
		112	833	1004-W0
14-in.	I	112	842	1004-W5
		113	841	1002-W5

Table 2 (cont'd)

Pipe	I/O	Descriptor	Node	Weld no.
16-in.	I	Main	696	CW-1/EXT
20-in.	I	Venturi	722	1007-W3
		Main	717	1007-W19
10-in.	O	110	786	1019-W2
		111	732	1005-W1
			799	1005-W2
			800	1005-W3
			804	1005-W6
			808	1005-W8
		112	735	1003-W1
			812	1003-W2
			821	1003-W8
		113	749	1001-W8
14-in.	O	110	797	1019-W12
		111	810 810	1005-W10 1005-W11
			811	1005-W12
		112	823 823	1003-W10 1003-W11
			824	1003-W12
		113	751 751	1001-W10 1001-W11

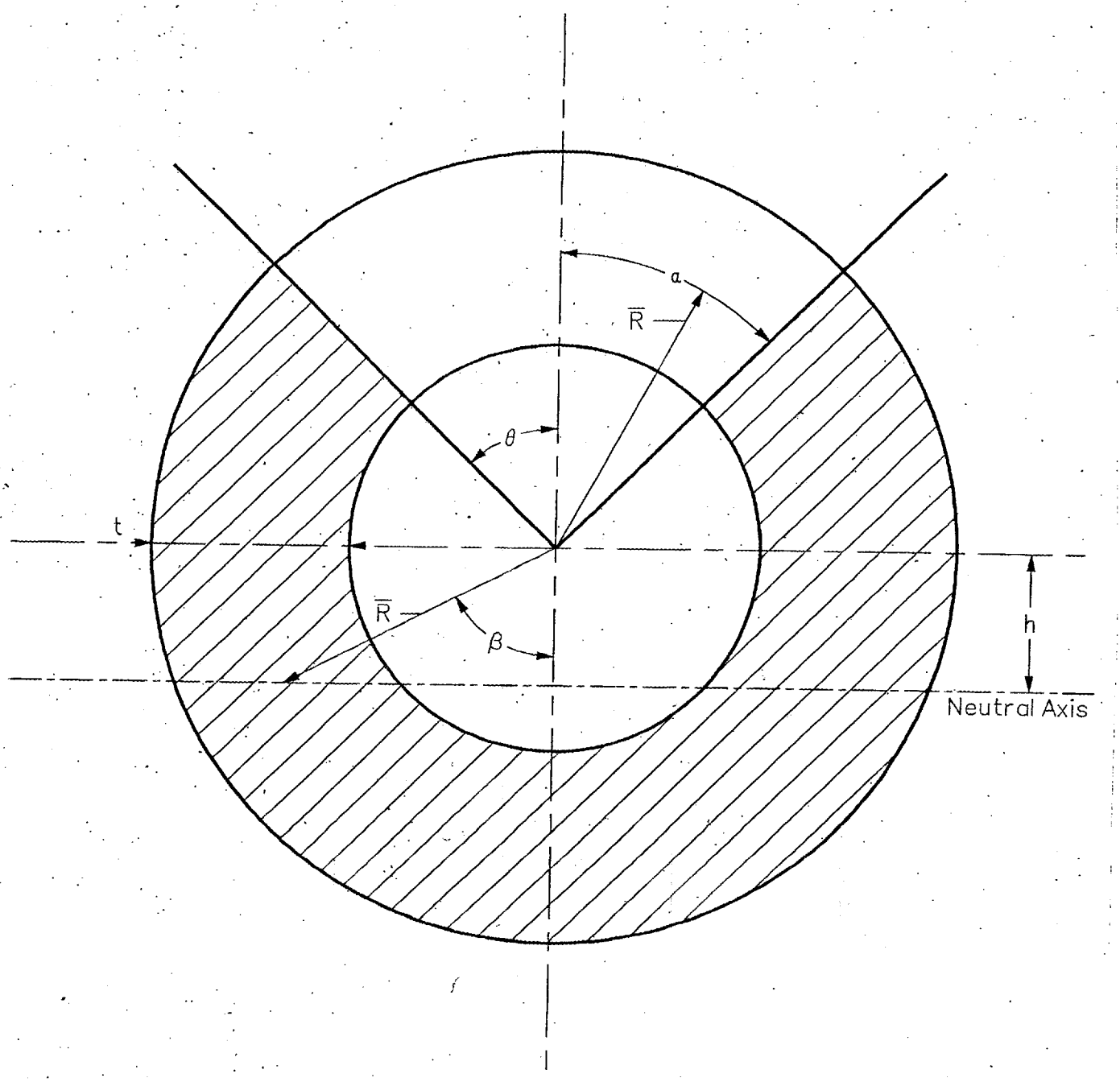

Fig. 1. Circumferential through-wall crack.

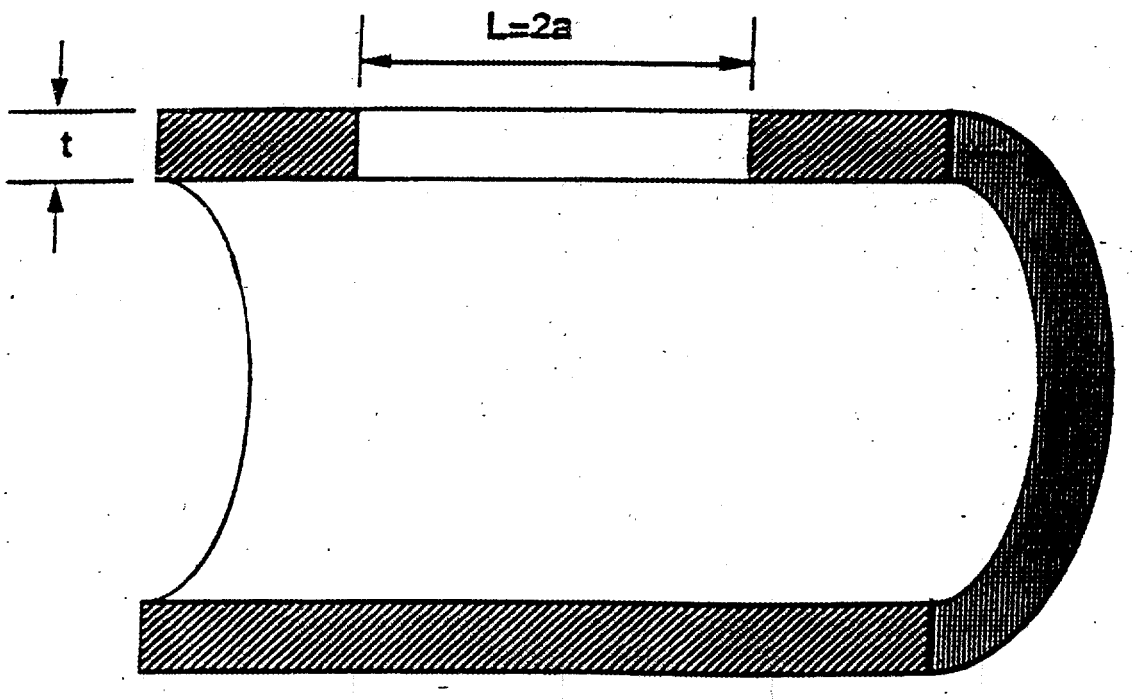

Fig. 2. Axial through-wall crack.

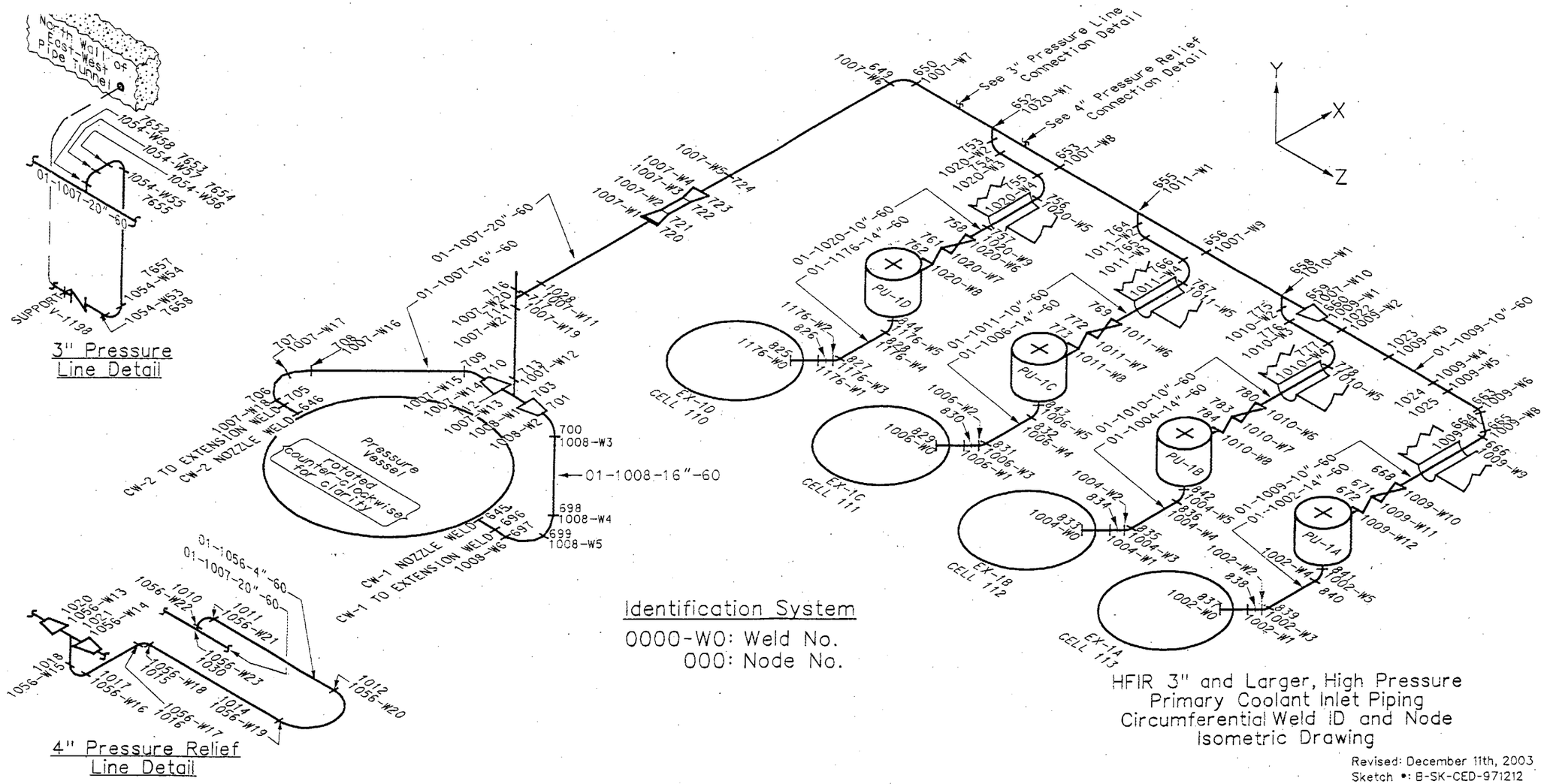
North wall of East-West Pipe Tunnel
3" Pressure Line Detail
4" Pressure Relief Line Detail
See 3" Pressure Line Connection Detail
See 4" Pressure Relief Connection Detail
Pressure Vessel
rotated counter-clockwise for clarity
CW-2 TO EXTENSION WELD
CW-2 NOZZLE WELD
CW-1 NOZZLE WELD
CW-1 TO EXTENSION WELD
SUPPORT
PU-1D
PU-1C
PU-1B
PU-1A
EX-1D CELL 110
EX-1C CELL 111
EX-1B CELL 112
EX-1A CELL 113
Identification System
0000-W0: Weld No.
000: Node No.
HFIR 3" and Larger, High Pressure Primary Coolant Inlet Piping Circumferential Weld ID and Node Isometric Drawing
Revised: December 11th, 2003
Sketch #: B-SK-CED-971212

Fig. 3.

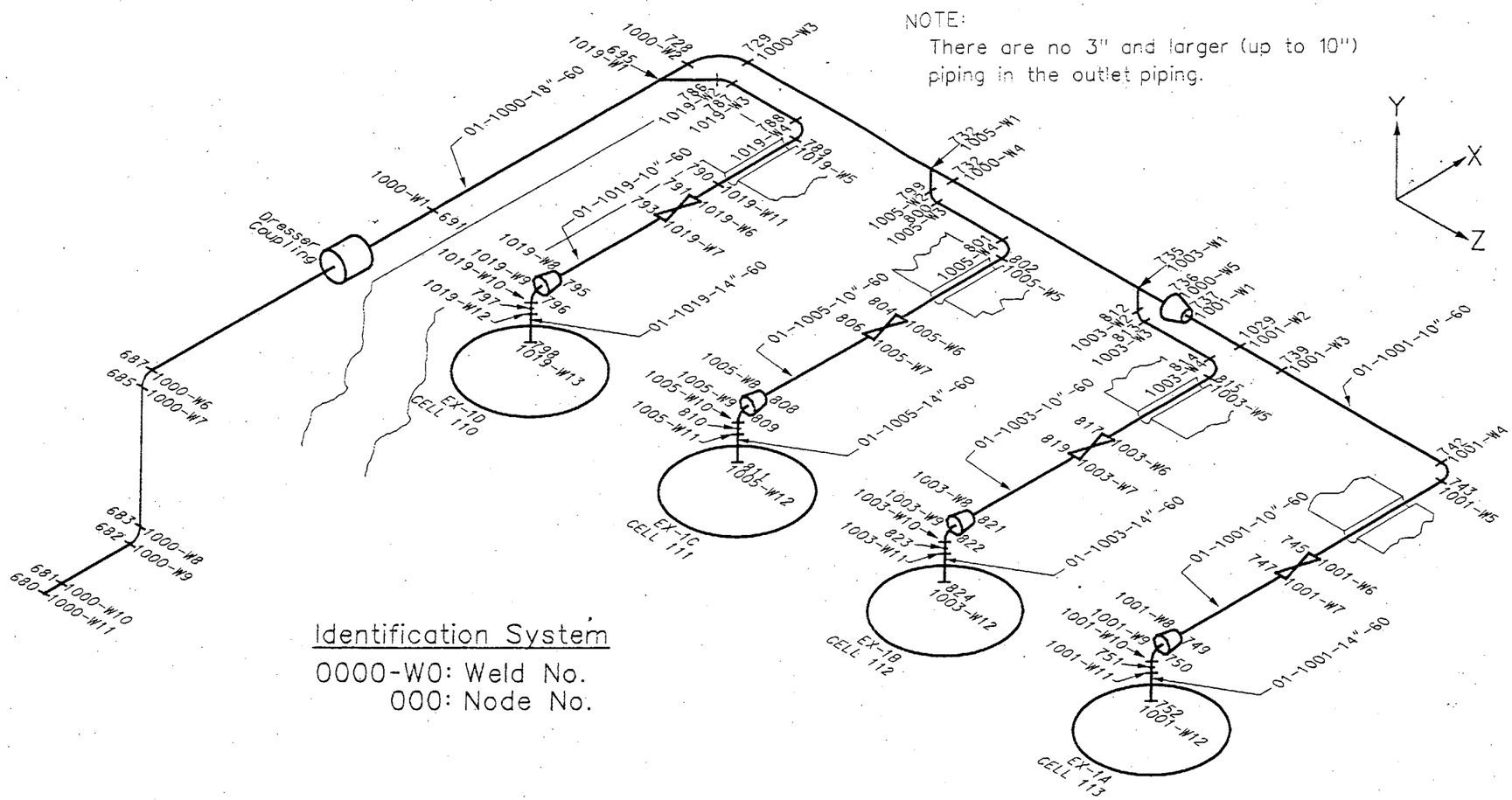

HFIR 10" and Larger, High Pressure Primary Coolant Outlet Piping Circumferential Weld ID and Node Isometric Drawing

Revised: December 11th, 2003

Fig. 4.

Appendix A

Calculation of $\sigma(HT)$, $\sigma(E/F)$, and $\sigma(S)$ for Primary-System 3-in. and larger Pipe and Components

A.1 Input

Input for calculation of the stresses for the welds in the HFIR primary-system 3-in. and larger pipe is provided in Table A1 (dimensional data), Table A2 (axial forces and bending moments due to constrained thermal expansion), and Table A3 (axial forces and bending moments for seismic events). Primary-system pressures included in the analysis are (1) hydro-test pressure of 900 psi; (2) emergency/faulted-condition (*E/F*) main circulating-pump discharge pressure at the time of rupture-disc failure with full flow (690 psi); (3) *E/F*-condition vessel discharge pressure of 580 psi, which is the maximum "normal-operation" pressure that could be experienced at vessel discharge with pony-motor flow; (4) normal operating pressure of 520 psi at the pump discharge; and (5) normal operating pressure of 470 psi at the vessel discharge. Items (2) and (4) are used for the *E/F* and seismic events, respectively, between pump discharge and vessel inlet, and items (3) and (5) are used for the *E/F* and seismic events between the vessel discharge and pump inlet.

Table A1. Dimensional data for HFIR piping and components

Pipe/ component	D_o (in.)	D_i (in.)	t (in.)	$\overline{R}$ (in.)	$\overline{R}/t$ (in.)	Z (in.)^3	h^a (in.)
3-in.	3.5	3.068	0.216	1.64	7.60	1.724	0.57
4-in.	4.50	4.03	0.237	2.13	9.00	3.21	0.566
10-in.	10.75	10.02	0.365	5.19	14.20	29.90	0.550
14-in.[b]	14.00	11.70	1.150	6.43	5.59	138	0.50
14-in.	14.00	13.12	0.438	6.78	15.48	61.61	0.509
16-in.	16.00	15.00	0.500	7.75	15.50	91.49	0.506
18-in.	18.00	16.92	0.538	8.73	16.23	125.5	0.503
20-in.	20.00	18.81	0.596	9.70	16.28	170.9	0.501
CV/GV[c]	10.75	9.90	0.425	5.16	12.1	34.2	0.519
P/CV[d]	10.75	9.81	0.468	5.14	11.0	37.4	0.519
Venturi	16.88	15.18	0.850	8.02	9.43	163	0.505
VLE[e]	36.00	33.00	1.500	17.25	11.5	1.35×10^3	0.491
HX[f]	49.90	47.00	1.450	24.23	16.71	2.60×10^3	0.448

[a]Corresponds to 3.0-in.-long through-wall flaw.
[b]Nodes 841, 842, 843, 844.
[c]Check-valve/gate-valve juncture.
[d]Pump/check-valve juncture.
[e]Vessel lower extension bimetallic weld.
[f]Heat-exchanger head-to-tube-sheet bimetallic weld.

Table A2. Forces and moments for HFIR primary piping welds: constrained-thermal-expansion loads

				Constrained-thermal-expansion loads		
"Branch"	Node[a]	Element[a]	Weld type[b]	F(axial) (lbs)	M(y) (lb-in.)	M(z) (lb-in.)
3-in., I	7652	702	NF	1.36e+02	-1.56e+03	1.20e+03
	7653	703	NF	-1.20e+02	1.53e+03	-2.71e+03
	7654	703	NF	-1.20e+02	1.30e+03	-3.85e+03
	7655	705	NF	-1.36e+02	4.39e+02	-4.08e+03
	7657	706	NF	-1.36e+02	2.03e+02	3.65e+03
	7658	707	NF	3.74e+00	4.28e+02	6.33e+02
4-in., I	1030	445	NF	-2.69e-01	3.48e+02	3.68e+01
	1010	445	NF	-2.69e-01	3.00e+02	3.40e+01
	1011	447	NF	-4.52e+00	1.85e+00	3.93e+02
	1012	447	NF	-4.52e+00	1.46e+01	3.93e+02
	1014	450	NF	4.52e+00	-1.46e+01	3.34e+02
	1015	450	NF	4.52e+00	-1.85e+00	3.34e+02
	1016	452	NF	6.88e-04	3.05e+02	2.51e+01
	1017	452	NF	6.88e-04	3.09e-11	-5.04e-09
	1018	454	NF	0.00e+00	3.07e-11	-5.72e-10
	1020	456	NF	1.46e-11	-1.31e-10	9.71e-11
	1021	456	NF	1.46e-11	-4.00e-11	-2.27e-13
10-in., I, 110	652	323	NF	6.80e+02	7.12e+04	2.61e+03
	753	323	F	6.80e+02	5.13e+04	1.45e+03
	754	325	F	-2.59e+01	-4.07e+04	-1.93e+03
	755	325	F	-2.59e+01	8.55e+03	1.61e+02
	756	327	NF	9.88e+02	-2.38e+04	-1.13e+03
	757	328	NF	9.88e+02	-2.52e+04	-3.40e+03
	758	328	NF	9.88e+02	-2.61e+04	-4.95e+03
	761	107	NF	9.88e+02	2.29e+03	-2.69e+04

Table A2 (cont'd)

				Constrained-thermal-expansion loads		
"Branch"	Node[a]	Element[a]	Weld type[b]	F(axial) (lbs)	M(y) (lb-in.)	M(z) (lb-in.)
10-in., I, 110	762	106	NF	9.88e+02	7.89e+03	-2.75e+04
14-in, I, 110	844	389	F	-1.41e+04	8.02e+05	-2.60e+04
	828	376	NF	-7.60e+04	-3.97e+04	4.97e+05
	827	376	NF	-7.60e+04	1.54e+05	-4.12e+04
Flange pair	826	374	NF	-5.73e+04	-2.38e+05	-1.82e+05
	826	375	F	-5.73e+04	2.38e+05	1.82e+05
	825	374	NF	-5.73e+04	-5.96e+05	-2.83e+05
10-in., I, 111	655	329	NF	-2.21e+02	4.30e+04	2.55e+03
	764	329	F	-2.21e+02	2.90e+04	1.48e+03
	765	331	F	-5.14e+02	-2.46e+04	-2.07e+03
	766	331	F	-5.14e+02	-1.32e+04	1.13e+02
	767	333	NF	2.02e+02	2.42e+03	-1.15e+03
	769	334	NF	2.02e+02	-4.43e+04	-4.67e+03
	772	120	NF	2.02e+02	1.74e+03	-6.03e+04
	773	119	NF	2.02e+02	6.71e+03	-7.26e+04
14-in., I, 111	843	388	F	-1.43e+04	7.97e+05	-3.23e+04
	832	379	NF	-7.62e+04	-5.23e+04	5.02e+05
	831	379	F	-7.62e+04	1.56e+05	-4.33e+04
Flange pair	830	377	F	-5.77e+04	-2.31e+05	-1.85e+05
	830	378	F	-5.77e+04	2.31e+05	1.85e+05
	829	377	F	-5.77e+04	-5.88e+05	-2.87e+05
10-in., I, 112	658	335	NF	-7.60e+02	3.90e+04	2.50e+03
	775	335	F	-7.60e+02	2.39e+04	1.44e+03

Table A2 (cont'd)

				Constrained-thermal-expansion loads		
"Branch"	Node[a]	Element[a]	Weld type[b]	F(axial) (lbs)	M(y) (lb-in.)	M(z) (lb-in.)
10-in., I, 112	776	337	F	-9.22e+02	-2.15e+04	-2.05e+03
	777	337	F	-9.22e+02	-3.01e+04	1.05e+02
	778	339	NF	-1.53e+02	1.86e+04	-1.17e+03
	780	340	NF	-1.53e+02	-6.53e+04	-4.65e+03
	783	133	NF	-1.53e+02	1.80e+03	-9.39e+04
	784	132	NF	-1.53e+02	6.79e+03	-1.16e+05
14-in., I, 112	842	387	F	-1.42e+04	7.86e+05	-3.62e+04
	836	382	NF	-7.54e+04	-5.93e+04	4.99e+05
	835	382	F	-7.54e+04	1.57e+05	-4.29e+04
Flange pair	834	380	F	-5.50e+04	-2.22e+05	-1.74e+05
	834	381	F	-5.73e+04	2.22e+05	1.83e+05
	833	380	F	-5.50e+04	-6.11e+05	-2.81e+05
10-in., I, 113	660	287	F	-1.00e+03	1.76e+04	1.19e+03
	1022	287	F	-1.00e+03	9.51e+03	2.99e+02
	1023	288	F	-1.00e+03	-7.55e+03	-1.58e+03
	1024	290	F	-1.00e+03	-2.43e+04	-2.37e+03
	1025	291	F	-1.00e+03	-2.77e+04	-2.00e+03
	663	293	F	-1.00e+03	-4.44e+04	-2.12e+02
	664	295	F	-9.11e+02	4.30e+04	-2.97e+02
	665	295	F	-9.11e+02	3.20e+04	-9.53e+02
	666	297	NF	-2.84e+02	2.26e+04	-1.10e+03
	668	298	NF	-2.84e+02	-7.76e+04	-4.15e+03
	671	146	NF	-2.84e+02	2.00e+03	-1.09e+05
	672	145	NF	-2.84e+02	6.77e+03	-1.33e+05

Table A2 (cont'd)

				Constrained-thermal-expansion loads		
"Branch"	Node[a]	Element[a]	Weld type[b]	F(axial) (lbs)	M(y) (lb-in.)	M(z) (lb-in.)
14-in., I, 113	841	386	F	-1.44e+04	7.93e+05	-3.52e+04
	840	385	NF	-7.61e+04	-5.88e+04	5.03e+05
	839	385	F	-7.61e+04	1.57e+05	-4.42e+04
Flange pair	838	383	F	-5.78e+04	-2.27e+05	-1.85e+05
	838	384	F	-5.78e+04	2.27e+05	1.85e+05
	837	383	NF	-5.78e+04	-5.82e+05	-2.88e+05
16-in., I	696	242	F	1.94e+03	5.52e+04	-7.04e+03
	697	243	NF	1.94e+03	5.34e+04	-8.56e+03
	699	244	F	-1.15e+02	2.05e+04	1.77e+04
	698	246	NF	-1.45e+03	8.95e+02	-1.86e+04
	700	246	NF	-1.45e+03	8.07e+04	-1.25e+04
	701	248	F	-1.88e+03	8.85e+04	-1.91e+03
	705	249	F	1.79e+03	6.56e+04	-3.17e+03
	706	250	NF	1.79e+03	5.32e+04	7.85e+03
	707	251	F	7.01e+02	3.57e+04	-1.36e+04
	708	253	NF	-1.84e+03	-4.89e+03	-2.46e+04
	709	253	NF	-1.84e+03	-4.82e+04	1.93e+04
	710	255	F	-1.62e+03	4.76e+04	-2.02e+04
20-in., I	712	256	F	-1.79e+03	2.71e+04	-3.62e+04
	703	257	F	-1.94e+03	8.03e+04	-2.61e+03
	713	258	NF	-8.10e+02	2.66e+04	-4.26e+04
	714	259	F	-8.10e+02	1.41e+04	-5.99e+04
	716	261	F	-4.66e-10	1.16e-09	1.51e-09

Table A2 (cont'd)

				Constrained-thermal-expansion loads		
"Branch"	Node[a]	Element[a]	Weld type[b]	F(axial) (lbs)	M(y) (lb-in.)	M(z) (lb-in.)
20-in., I	717	262	F	-7.52e+02	5.42e+04	-5.80e+04
	1028	263	NF	-7.52e+02	4.61e+04	-4.60e+04
	720	266	F	-7.52e+02	-2.22e+04	5.56e+04
	721	267	F	-7.52e+02	-2.98e+04	6.65e+04
	722	269	F	-7.52e+02	-4.94e+04	6.66e+04
	723	269	F	-7.52e+02	-5.71e+04	5.49e+04
	724	270	NF	-7.52e+02	-3.83e+04	2.43e+04
	649	274	NF	-7.52e+02	-8.08e+03	-4.54e+00
	650	275	F	-2.47e+03	-5.97e+04	1.27e+03
	653	279	F	-2.44e+03	1.74e+03	-5.71e+04
	656	282	NF	-1.93e+03	3.71e+04	-9.14e+01
	659	285	F	-1.00e+03	2.22e+04	1.69e+03
10-in., O, 110	695	341	NF	-5.77e+02	-7.35e+04	3.55e+03
	786	341	F	-5.77e+02	-5.29e+04	6.25e+03
	787	343	NF	1.09e+01	-4.41e+04	-3.48e+03
	788	344	F	1.09e+01	4.59e+03	6.41e+03
	789	345	NF	8.03e+02	-1.65e+04	6.10e+03
	790	346	NF	8.03e+02	-1.59e+04	-5.63e+03
	791	346	NF	8.03e+02	-1.56e+04	-1.21e+04
	793	347	NF	8.03e+02	-1.52e+04	6.65e+04
	795	348	NF	8.03e+02	-1.42e+04	-1.88e+05
14-in., O, 110	796	349	NF	8.03e+02	-1.40e+04	1.73e+04
Flange pair	797	350	NF	5.74e+02	-1.88e+04	2.41e+05
	797	351	F	5.69e+02	-1.88e+04	2.40e+05
	798	351	NF	5.69e+02	-2.27e+04	3.47e+05

Table A2 (cont'd)

				Constrained-thermal-expansion loads		
"Branch"	Node[a]	Element[a]	Weld type[b]	F(axial) (lbs)	M(y) (lb-in.)	M(z) (lb-in.)
10-in., O, 111	732	352	NF	3.09e+02	4.23e+04	7.09e+03
	799	352	F	3.09e+02	3.70e+04	4.56e+03
	800	354	F	-2.06e+02	-3.23e+04	4.80e+02
	801	355	F	-2.06e+02	-1.10e+04	8.08e+03
	802	356	NF	3.54e+02	2.62e+03	2.06e+03
	804	357	NF	3.54e+02	-1.47e+04	-8.28e+03
	806	358	NF	3.54e+02	-2.10e+04	6.70e+04
	808	359	F	3.54e+02	-4.06e+04	-1.90e+05
14-in., O, 111	809	360	F	3.54e+02	-4.33e+04	1.77e+04
Flange pair	810	361	F	1.04e+02	-4.85e+04	2.44e+05
	810	362	F	1.01e+02	-4.85e+04	2.43e+05
	811	362	F	1.01e+02	-5.13e+04	3.52e+05
10-in., O, 112	735	363	NF	-3.69e+02	3.25e+04	4.88e+03
	812	363	F	-3.69e+02	2.53e+04	2.25e+03
	813	365	NF	-4.44e+02	-2.41e+04	1.42e+03
	814	366	F	-4.44e+02	-2.88e+04	7.43e+03
	815	367	NF	-7.73e+01	2.33e+04	1.29e+03
	817	368	NF	-7.73e+01	-1.40e+04	-9.27e+03
	819	369	NF	-7.73e+01	-2.78e+04	6.78e+04
	821	370	F	-7.73e+01	-7.01e+04	-1.92e+05
14-in., O, 112	822	371	F	-7.73e+01	-7.59e+04	1.88e+04
Flange pair	823	372	F	-3.70e+02	-8.21e+04	2.49e+05
	823	373	F	-3.40e+02	-8.21e+04	2.60e+05
	824	373	F	-3.40e+02	-8.39e+04	3.60e+05

Table A2 (cont'd)

				Constrained-thermal-expansion loads		
"Branch"	Node[a]	Element[a]	Weld type[b]	F(axial) (lbs)	M(y) (lb-in.)	M(z) (lb-in.)
10-in., O, 113	737	309	NF	-5.29e+02	9.30e+03	1.10e+03
	1029	309	F	-5.29e+02	3.68e+03	-2.06e+03
	739	311	F	-5.29e+02	-1.20e+04	-1.44e+02
	742	314	F	-5.29e+02	-4.21e+04	7.05e+03
	743	316	NF	-2.18e+02	3.75e+04	5.58e+02
	745	317	NF	-2.18e+02	-1.97e+04	-7.35e+03
	747	318	NF	-2.18e+02	-3.61e+04	6.72e+04
	749	319	F	-2.18e+02	-8.65e+04	-1.91e+05
14-in, O, 113	750	320	F	-2.18e+02	-9.34e+04	1.76e+04
	751	321	F	-5.29e+02	-9.99e+04	2.46e+05
	751	322	F	-5.30e+02	-9.99e+04	2.45e+05
	752	322	NF	-5.30e+02	-1.01e+05	3.54e+05
18-in., O	680	228	F	-7.20e+02	-2.34e+04	2.33e+04
	681	230	NF	-7.20e+02	-1.65e+04	2.95e+04
	682	230	NF	-7.20e+02	-1.41e+03	4.30e+04
	683	232	F	-4.41e+02	1.15e+04	3.78e+04
	685	232	NF	-4.41e+02	-3.25e+03	-5.88e+04
	687	233	NF	-8.62e+02	-7.01e+04	-8.32e+03
	691	238	F	-8.62e+02	-1.20e+04	1.92e+03
	728	299	NF	-1.05e+01	1.55e+04	2.82e+04
	729	301	F	-1.18e+03	-1.46e+04	-1.49e+04
	732	304	F	-9.73e+02	3.88e+04	-4.68e+03
	736	307	F	-5.29e+02	1.28e+04	3.06e+03

[a]Node and element numbers used in Refs. 10, 13, 18, and 19.
[b]Flux and non-flux welds.

Table A3. Forces and moments for HFIR primary piping welds: seismic loads

				Seismic loads		
"Branch"	Node[a]	Element[a]	Weld type[b]	F(axial) (lbs)	M(y) (lb-in.)	M(Z) (lb-in.)
3-in., I	7652	702	NF	5.53e+01	4.24e+02	9.10e+02
	7653	703	NF	1.13e+01	6.08e+02	1.44e+02
	7654	703	NF	1.13e+01	3.78e+02	3.42e+02
	7655	705	NF	5.53e+01	9.97e+02	3.61e+02
	7657	706	NF	5.52e+01	1.18e+03	5.72e+01
	7658	707	NF	3.64e+01	1.10e+03	2.81e+02
4-in., I	1030	445	NF	3.24e+02	8.43e+03	4.22e+03
	1010	445	NF	3.24e+02	7.49e+03	1.15e+03
	1011	447	NF	9.14e+01	8.85e+02	7.00e+03
	1012	447	NF	9.14e+01	1.59e+03	7.40e+03
	1014	450	NF	7.98e+01	1.58e+03	8.34e+03
	1015	450	NF	7.98e+01	4.44e+02	3.84e+03
	1016	452	NF	2.48e+02	5.22e+03	4.35e+02
	1017	452	NF	2.48e+02	2.43e+02	1.92e+03
	1018	454	NF	5.15e+00	1.99e+02	7.04e+02
	1020	456	NF	2.62e-12	1.22e+03	1.26e+02
	1021	456	NF	2.62e-12	6.57e-11	1.30e-12
10-in., I, 110	652	323	NF	1.29e+03	1.09e+05	2.73e+03
	753	323	F	1.29e+03	8.43e+04	1.37e+03
	754	325	F	3.24e+02	6.91e+04	2.06e+03
	755	325	F	3.24e+02	1.14e+04	2.74e+03
	756	327	NF	1.62e+03	3.08e+04	1.38e+03
	757	328	NF	1.62e+03	1.40e+04	1.57e+03
	758	328	NF	1.62e+03	8.23e+03	3.84e+03
	761	107	NF	1.66e+03	6.18e+03	1.39e+04
	762	106	NF	1.66e+03	1.07e+03	2.52e+04

Table A.3 (cont'd)

				Seismic loads		
"Branch"	Node[a]	Element[a]	Weld type[b]	F(axial) (lbs)	M(y) (lb-in.)	M(Z) (lb-in.)
14- in., I, 110	844	389	F	2.82e+02	2.95e+04	1.68e+04
	828	376	NF	2.04e+03	2.90e+04	1.12e+04
	827	376	NF	2.04e+03	7.99e+03	3.71e+03
Flange pair	826	374	NF	1.88e+03	1.65e+04	3.09e+03
	826	375	F	1.88e+03	1.65e+04	3.09e+03
	825	374	NF	1.88e+03	2.15e+04	4.07e+03
10-in., I, 111	655	329	NF	1.83e+03	1.47e+05	7.61e+03
	764	329	F	1.83e+03	1.17e+05	2.98e+03
	765	331	F	5.59e+02	9.63e+04	4.52e+03
	766	331	F	5.59e+02	3.29e+04	5.20e+03
	767	333	NF	2.33e+03	6.00e+04	3.45e+03
	769	334	NF	2.33e+03	1.43e+04	1.20e+04
	772	120	NF	2.39e+03	8.82e+03	2.02e+04
	773	119	NF	2.39e+03	1.51e+03	4.04e+04
14-in., I, 111	843	388	F	3.47e+02	2.34e+04	2.06e+04
	832	379	NF	1.71e+03	3.57e+04	1.14e+04
	831	379	F	1.71e+03	9.17e+03	3.45e+03
Flange pair	830	377	F	1.85e+03	1.94e+04	4.36e+03
	830	378	F	1.86e+03	1.94e+04	4.36e+03
	829	377	F	1.85e+03	2.16e+04	5.61e+03
10-in., I, 112	658	335	NF	1.71e+03	1.30e+05	3.76e+03
	775	335	F	1.71e+03	1.03e+05	1.57e+03
	776	337	F	5.60e+02	8.44e+04	2.66e+03
	777	337	F	5.60e+02	3.68e+04	3.59e+03
	778	339	NF	2.19e+03	6.17e+04	1.98e+03

Table A.3 (cont'd)

				Seismic loads		
"Branch"	Node[a]	Element[a]	Weld type[b]	F(axial) (lbs)	M(y) (lb-in.)	M(Z) (lb-in.)
10-in., I, 112	780	340	NF	2.20e+03	1.23e+04	6.77e+03
	783	133	NF	2.25e+03	5.44e+03	2.24e+04
	784	132	NF	2.25e+03	1.34e+03	4.32e+04
14-in., I, 112	842	387	F	3.16e+02	2.01e+04	1.77e+04
	836	382	NF	1.47e+03	3.07e+04	1.02e+04
	835	382	F	1.47e+03	7.85e+03	3.13e+03
Flange pair	834	380	F	1.56e+03	1.67e+04	3.93e+03
	834	381	F	1.60e+03	1.67e+04	4.12e+03
	833	380	F	1.56e+03	1.86e+04	5.21e+03
10-in., I, 113	660	287	F	3.48e+02	2.83e+04	1.74e+03
	1022	287	F	3.48e+02	3.23e+04	1.02e+03
	1023	288	F	3.24e+02	3.22e+04	3.95e+03
	1024	290	F	2.94e+02	1.80e+04	4.70e+03
	1025	291	F	2.94e+02	1.44e+04	4.13e+03
	663	293	F	2.88e+02	1.71e+04	4.99e+03
	664	295	F	4.94e+02	2.06e+04	3.15e+03
	665	295	F	4.94e+02	2.43e+04	4.12e+03
	666	297	NF	5.04e+02	2.46e+04	1.03e+03
	668	298	NF	5.09e+02	1.62e+04	1.00e+04
	671	146	NF	5.81e+02	6.03e+03	1.51e+04
	672	145	NF	5.81e+02	1.08e+03	3.06e+04
14-in., I, 113	841	386	F	2.75e+02	2.51e+04	1.47e+04
	840	385	NF	1.69e+03	2.57e+04	9.81e+03

Table A.3 (cont'd)

				Seismic loads		
"Branch"	Node[a]	Element[a]	Weld type[b]	F(axial) (lbs)	M(y) (lb-in.)	M(Z) (lb-in.)
14-in., I, 113	839	385	F	1.69e+03	6.88e+03	3.53e+03
Flange pair	838	383	F	1.58e+03	1.47e+04	3.62e+03
	838	384	F	1.57e+03	1.47e+04	3.62e+03
	837	383	NF	1.58e+03	1.87e+04	4.63e+03
16-in., I	696	242	F	3.23e+03	1.20e+05	1.56e+04
	697	243	NF	3.23e+03	7.33e+04	6.07e+03
	699	244	F	3.21e+03	3.09e+04	1.79e+04
	698	246	NF	4.63e+03	5.11e+04	1.01e+04
	700	246	NF	4.63e+03	7.99e+04	8.46e+04
	701	248	F	2.78e+03	7.10e+04	2.91e+04
	705	249	F	7.78e+02	1.19e+04	1.86e+04
	706	250	NF	7.78e+02	2.10e+04	2.12e+04
	707	251	F	1.13e+03	2.63e+04	1.79e+04
	708	253	NF	4.17e+02	1.05e+04	1.26e+04
	709	253	NF	4.17e+02	7.84e+04	1.73e+04
	710	255	F	1.14e+03	9.81e+04	1.83e+04
20-in., I	712	256	F	8.75e+02	1.21e+05	1.93e+04
	703	257	F	3.57e+03	7.13e+04	6.54e+04
	713	258	NF	1.15e+03	2.34e+04	7.20e+04
	714	259	F	1.15e+03	1.27e+04	1.29e+05
	716	261	F	9.79e-11	2.36e-10	4.29e-10
	717	262	F	6.55e+03	1.52e+05	1.93e+05
	1028	263	NF	6.55e+03	1.38e+05	1.76e+05

Table A.3 (cont'd)

				Seismic loads		
"Branch"	Node[a]	Element[a]	Weld type[b]	F(axial) (lbs)	M(y) (lb-in.)	M(Z) (lb-in.)
20-in., I	720	266	F	7.12e+03	5.36e+04	3.03e+04
	721	267	F	7.12e+03	7.63e+04	2.39e+04
	722	269	F	7.12e+03	1.37e+05	3.48e+04
	723	269	F	7.12e+03	1.62e+05	3.73e+04
	724	270	NF	7.29e+03	1.41e+05	1.58e+04
	649	274	NF	7.73e+03	1.81e+05	4.89e+03
	650	275	F	2.27e+03	1.10e+05	9.78e+03
	653	279	F	1.70e+03	3.49e+03	1.93e+05
	656	282	NF	1.05e+03	1.63e+05	5.16e+03
	659	285	F	4.23e+02	2.47e+04	2.71e+03
10-in., O, 110	695	341	NF	3.79e+02	1.84e+04	9.01e+03
	786	341	F	3.79e+02	9.92e+03	4.71e+03
	787	343	NF	5.93e+02	1.08e+04	5.40e+03
	788	344	F	5.86e+02	1.27e+04	1.14e+04
	789	345	NF	1.54e+02	5.31e+03	4.07e+03
	790	346	NF	1.56e+02	2.54e+04	2.46e+03
	791	346	NF	1.56e+02	4.07e+04	5.79e+03
	793	347	NF	4.59e+02	4.02e+04	3.35e+03
	795	348	NF	4.65e+02	1.64e+04	9.57e+03
14-in., O, 110	796	349	NF	4.69e+02	2.46e+04	3.30e+03
Flange pair	797	350	NF	5.03e+02	3.48e+04	1.25e+04
	797	351	F	5.04e+02	3.48e+04	1.25e+04
	798	351	NF	5.04e+02	3.85e+04	1.61e+04

Table A.3 (cont'd)

				Seismic loads		
"Branch"	Node[a]	Element[a]	Weld type[b]	F(axial) (lbs)	M(y) (lb-in.)	M(Z) (lb-in.)
10-in., O, 111	732	352	NF	9.83e+02	6.36e+04	8.87e+03
	799	352	F	9.83e+02	5.80e+04	4.68e+03
	800	354	F	7.94e+02	4.85e+04	3.43e+03
	801	355	F	7.74e+02	1.75e+04	1.49e+04
	802	356	NF	1.04e+03	2.66e+04	2.56e+03
	804	357	NF	1.04e+03	5.89e+04	6.90e+03
	806	358	NF	1.08e+03	5.59e+04	4.32e+03
	808	359	F	1.09e+03	2.68e+04	1.23e+04
14-in., O, 111	809	360	F	1.09e+03	3.86e+04	4.31e+03
Flange pair	810	361	F	1.06e+03	5.15e+04	1.56e+04
	810	362	F	1.06e+03	5.15e+04	1.57e+04
	811	362	F	1.06e+03	5.57e+04	1.98e+04
10-in., O, 112	735	363	NF	8.10e+02	7.75e+04	6.31e+03
	812	363	F	8.10e+02	5.76e+04	2.39e+03
	813	365	NF	6.45e+02	4.75e+04	3.59e+03
	814	366	F	6.32e+02	1.90e+04	1.27e+04
	815	367	NF	1.09e+03	3.26e+04	2.03e+03
	817	368	NF	1.09e+03	5.57e+04	6.16e+03
	819	369	NF	1.20e+03	5.09e+04	4.05e+03
	821	370	F	1.20e+03	2.71e+04	1.15e+04
14-in., O, 112	822	371	F	1.20e+03	3.81e+04	3.92e+03
Flange pair	823	372	F	1.22e+03	4.78e+04	1.43e+04
	823	373	F	1.25e+03	4.78e+04	1.41e+04
	824	373	F	1.25e+03	5.05e+04	1.85e+04

Table A.3 (cont'd)

				Seismic loads		
"Branch"	Node[a]	Element[a]	Weld type[b]	F(axial) (lbs)	M(y) (lb-in.)	M(Z) (lb-in.)
10-in., O, 113	737	309	NF	6.24e+02	1.82e+04	5.82e+03
	1029	309	F	6.24e+02	2.17e+04	4.75e+03
	739	311	F	5.88e+02	2.52e+04	3.65e+03
	742	314	F	5.24e+02	1.32e+04	9.90e+03
	743	316	NF	3.23e+02	1.40e+04	1.60e+03
	745	317	NF	3.25e+02	4.97e+04	3.99e+03
	747	318	NF	4.49e+02	4.51e+04	3.45e+03
	749	319	F	4.53e+02	2.47e+04	9.79e+03
14-in., O, 113	750	320	F	4.55e+02	3.47e+04	3.51e+03
	751	321	F	6.75e+02	4.59e+04	1.23e+04
	751	322	F	6.78e+02	4.59e+04	1.23e+04
	752	322	NF	6.78e+02	4.94e+04	1.61e+04
18-in., O	680	228	F	3.63e+02	2.02e+04	7.76e+04
	681	230	NF	4.06e+02	2.11e+04	7.17e+04
	682	230	NF	4.06e+02	2.40e+04	6.67e+04
	683	232	F	7.64e+02	5.62e+04	6.08e+04
	685	232	NF	7.64e+02	8.94e+03	2.93e+04
	687	233	NF	8.60e+02	4.48e+04	2.26e+04
	691	238	F	1.00e+03	7.69e+04	6.09e+04
	728	299	NF	1.19e+03	5.64e+04	1.59e+04
	729	301	F	2.19e+03	4.90e+04	1.29e+04
	732	304	F	1.35e+03	3.63e+04	1.07e+04
	736	307	F	6.24e+02	1.55e+04	7.18e+03

[a]Node and element numbers used in Refs. 10, 13, 18, and 19.
[b]Flux and non-flux welds.

A.2 Calculations

Values of, $\sigma(H/T)$, $\sigma(E/F)$, and $\sigma(S)$ were calculated for each of the welds identified in Table 1, and the results are presented in Table A4 for the non-flux welds and Table A5 for the flux-type welds. These tables also identify the welds for which $\sigma(HT) < \sigma(E/F)$ and $\sigma(HT) < \sigma(S)$. These are the welds for which hydro testing is not a satisfactory means of demonstrating structural integrity.

A sample calculation is included below for Node 843, which is at the attachment of a 14-in., 90° elbow ($D_i = 11.70$ in.) to the inlet of the pump in Branch III.

The values of $\sigma(HT)$, $\sigma(E/F)$, and $\sigma(S)$ are calculated using Eqs. (20), (21), and (22), leaving out the third terms. Thus,

$$\sigma(HT) = \frac{p(HT)}{2}\left(\frac{\overline{R}}{t}\right) + \frac{p(HT)\pi D_i^2 h}{4Z}$$

$$= \frac{900}{2} \times 5.59 + \frac{900\pi(11.7)^2 \times 0.5}{4 \times 138}$$

$$= 2.52 \times 10^3 + 0.35 \times 10^3 = 2.87 \times 10^3 \ psi$$

$$\sigma(E/F) = \frac{p(E/F)}{2}\left(\frac{\overline{R}}{t}\right) + \frac{p(E/F)\pi D_i^2 h}{4Z}$$

$$+ 1.8\left\{\frac{1}{Z}\left[M_e(y)^2 + M_e(z)^2\right]^{1/2} + \frac{F_e h}{Z} + \frac{4F_e}{\pi\left(D_o^2 - D_i^2\right)}\right\}$$

$$= \frac{580}{2} \times 5.59 + \frac{580\pi(11.7)^2 \times 0.5}{4 \times 138}$$

$$+ 1.8\left\{\frac{\left[(7.97 \times 10^5)^2 + (-3.23 \times 10^4)^2\right]^{1/2}}{138} - \frac{1.43 \times 10^4 \times 0.5}{138} - \frac{4 \times 1.43 \times 10^4}{\pi(14^2 - 11.7^2)}\right\}$$

$$= 1.62 \times 10^3 + 0.23 \times 10^3 + 9.76 \times 10^3 = 11.6 \times 10^3 \ psi$$

$$\sigma(S) = \frac{p(N)}{z}\left(\frac{\bar{R}}{t}\right) + \frac{p(N)\pi D_i^2 h}{4Z}$$

$$+ 1.8\left\{\frac{1}{Z}\left[\left(|M_e(y)| + M_s(y)\right)^2 + \left(|M_e(z)| + M_s(z)\right)^2\right]^{1/2} + \frac{(F_e + F_s)h}{Z} + \frac{4(F_e + F_s)}{\pi(D_o^2 - D_i^2)}\right\}$$

$$= \frac{470}{2} \times 5.59 + \frac{470\pi(11.7)^2 \times 0.50}{4 \times 138}$$

$$+ 1.8\left\{\frac{\left[(7.97 \times 10^5 + 2.34 \times 10^4)^2 + (3.23 \times 10^4 + 2.06 \times 10^4)^2\right]^{1/2}}{138}\right.$$

$$\left. + \frac{(-1.43 \times 10^4 + 3.47 \times 10^2) \times 0.50}{138} + \frac{4(-1.43 \times 10^4 + 3.47 \times 10^2)}{\pi(14.00^2 - 11.70^2)}\right\}$$

$$= 1.32 \times 10^3 + 0.18 \times 10^3 + 10.08 \times 10^3 = 11.6 \times 10^3 \; psi$$

For the hydro test to be an appropriate demonstration of structural integrity, Eq. (10) must be satisfied. The required condition is

$$(\sigma_b + \sigma_m)(HT) \geq (\sigma_b + \sigma_m)(WC) \qquad \textbf{(10)}$$

From the above calculations,

$$\frac{\sigma(HT)}{\sigma(E/F)} = \frac{2.87 \times 10^3}{11.7 \times 10^3} = 0.25 < 1.0$$

$$\frac{\sigma(HT)}{\sigma(S)} = \frac{2.87 \times 10^3}{11.7 \times 10^3} = 0.25 < 1.0$$

It is apparent that Eq. (10) is not satisfied, and thus hydro testing is not an appropriate means of demonstrating the structural integrity of the particular weld (node 843).

Table A4. σ(*HT*) and σ(*S*) for non-flux welds in HFIR primary-system 3-in and larger piping

Pipe	I/O[a]	Descriptor[a]	Node[a]	*p(N)* [psi]	σ(*HT*), [ksi]	σ(*S*) [ksi]	σ(*S*) > σ(*HT*)? [Y]
3-in.	I	PL	7652	520	5.6	4.4	
			7653			3.9	
			7654			3.8	
			7655			4.4	
			7657			4.6	
			7658			4.5	
4-in.	I	PR	1030	520	6.1	9.1	Y
			1010			8.0	Y
			1011			7.5	Y
			1012			7.8	Y
			1014			8.3	Y
			1015			5.7	
			1016			6.7	Y
			1017			4.8	
			1018			3.9	
			1020			4.2	
			1021			3.5	
10-in.	I	110	652	520	7.7	11.2	Y
			756			6.6	
			757			5.6	
			758			5.3	
			761		6.5	4.8	
			762		5.9	4.8	
		111	655		7.7	13.6	Y

Table A4 (cont.'d)

Pipe	I/O[a]	Descriptor[a]	Node[a]	*p(N)* [psi]	σ(*HT*), [ksi]	σ(*S*) [ksi]	σ(*S*) > σ(*HT*)? [Y]
10-in.	I	111	767	520	7.7	8.5	Y
			769			6.0	
			772		6.5	5.3	
			773		5.9	5.7	
		112	658		7.7	12.6	Y
			778			8.6	Y
			780			5.7	
			783		6.5	5.3	
			784		5.9	5.7	
		113	666		7.7	6.0	
			668			5.7	
			671		6.5	4.7	
			672		5.9	5.0	
14-in.	I	110	828	520	8.0	5.7	
			827			5.1	
			826			5.3	
			825			5.5	
		111	832			5.9	
		112	836			5.7	
		113	840			5.6	
14.-in.			837			5.3	

Table A4 (cont.'d)

Pipe	I/O[a]	Descriptor[a]	Node[a]	*p(N)* [psi]	σ(*HT*), [ksi]	σ(*S*) [ksi]	σ(*S*) > σ(*HT*)? [Y]
16-in.	I	Main	697	520	7.9	6.3	
			698			6.0	
			700			7.2	
			706			5.2	
			708			4.9	
			709			6.2	
20-in.	I	Main/Tee	713	520	8.1	5.5	
			1028			7.4	
			724			6.5	
			649			7.0	
			656			6.4	
10-in.	O	110	695	470	7.7	5.3	
			787			4.9	
			789			4.4	
			790			5.6	
			791			6.5	
			793			6.5	
			795			5.2	
		111	732			8.1	Y
			802			5.8	
			804			7.8	Y
			806			7.6	

Table A4 (cont.'d)

Pipe	I/O[a]	Descriptor[a]	Node[a]	*p(N)* [psi]	σ(*HT*), [ksi]	σ(*S*) [ksi]	σ(*S*) > σ(*HT*)? [Y]
10-in.	O	112	735	470	7.7	8.8	Y
			813			7.0	
			815			6.2	
			817			7.6	
			819			7.3	
		113	737			5.3	
			743			4.9	
			745			7.1	
			747			6.8	
14-in.	O	110	796	470	8.0	4.9	
			797			5.3	
			798			5.4	
		113	752			5.8	
18-in.	O	Main	681	470	8.1	5.3	
			682			5.3	
			685			4.7	
			687			5.0	
			728			5.2	

[a]See footnote to Table 1.

Table A5. σ(*HT*), σ(*E/F*) and σ(*S*) for flux-type welds in HFIR primary-system 3-in. and larger piping

Pipe	I/O[a]	Descriptor[a]	Node[a]	*p(E/F)* [psi]	*p(N)* [psi]	σ*(HT)* [ksi]	σ*(E/F)* [ksi]	σ(*E/F*) > σ(*HT*)? [Y]	σ(*S*) [ksi]	σ(*S*) > σ(*HT*)? [Y]
10-in.	I	110	753	690	520	7.7	9.2	Y	13.0	Y
			754				8.4	Y	11.2	Y
			755				6.4		5.7	
		111	764				7.6		13.6	Y
			765				7.3		11.8	Y
			766				6.6		7.3	
		112	775				7.2		12.3	Y
			776				7.0		10.8	Y
			777				7.6		8.4	Y
		113	660				6.8		7.1	
			1022				6.3		6.9	
			1023				6.2		6.7	
			1024				7.2		6.9	
			1025				7.4		6.9	
			663				8.4	Y	8.1	Y
			664				8.3	Y	8.2	Y
			665				7.7		7.8	Y
14-in.	I	110	844	580	470	2.9	11.6	Y	11.8	Y
			826			8.0	7.6		7.3	
		111	843			2.9	11.7	Y	11.6	Y
			831			8.0	1.4		0.9	

Table A5 (cont.'d)

Pipe	I/O[a]	Descriptor[a]	Node[a]	*p(E/F)* [psi]	*p(N)* [psi]	σ*(HT)* [ksi]	σ*(E/F)* [ksi]	σ(*E/F*) > σ(*HT*)? [Y]	σ(*S*) [ksi]	σ(*S*) > σ(*HT*)? [Y]
14-in.	I	Flange pair	830 830	580	470	8.0	7.4 7.4		7.2 7.2	
			829				17.8	Y	17.8	Y
		112	842			2.9	11.5	Y	11.5	Y
			835			8.0	1.5		0.9 7	
		Flange pair	834 834				7.3 7.3		7.0 7.0	
			833				18.8	Y	18.6	Y
		113	841			2.9	11.6	Y	11.6	Y
			839			8.0	1.5		0.9	
		Flange pair	838 838				7.3 7.3		6.9 6.9	
16-in.	I	Main	696	690	520	7.9	7.3		8.4	Y
			699				6.6		6.0	
			701				7.7		7.9	
			705				7.5		6.4	
			707				6.8		6.1	
			710				6.8		7.4	
20-in.	I	Main, Tee	703	690	520	8.1	7.0		6.5	
			712				6.5		6.2	
			714				6.8		6.7	

Table A5 (cont.'d)

Pipe	I/O[a]	Descriptor[a]	Node[a]	*p(E/F)* [psi]	*p(N)* [psi]	σ*(HT)* [ksi]	σ*(E/F)* [ksi]	σ(*E/F*) > σ(*HT*)? [Y]	σ(*S*) [ksi]	σ(*S*) > σ(*HT*)? [Y]
20-in.	I	Main	716	690	520	8.1	6.2		4.7	
			717				7.1		8.5	Y
			720				6.8		6.2	
		Ven	721			4.7	4.4		4.6	
			722				4.5		5.4	Y
			723			8.1	7.0		7.6	
			650				6.7		6.4	
			653				6.7		7.3	
			659				6.4		5.1	
10-in.	O	110	786	580	470	7.7	8.1	Y	7.8	Y
			788				5.4		5.6	
		111	799				7.3		10.0	Y
			800				6.9		9.0	Y
			801				5.8		6.4	
			808				16.7	Y	17.1	Y
		112	812				6.4		9.1	Y
			814				6.7		7.2	
			821				17.3	Y	17.8	Y
		113	1029				5.1		5.6	
			739				5.6		6.3	
			742				7.4		7.5	
			749				17.5	Y	17.9	Y

Table A5 (cont.'d)

Pipe	I/O[a]	Descriptor[a]	Node[a]	*p(E/F)* [psi]	*p(N)* [psi]	σ*(HT)* [ksi]	σ*(E/F)* [ksi]	σ(*E/F*) > σ(*HT*)? [Y]	σ(*S*) [ksi]	σ(*S*) > σ(*HT*)? [Y]
14-in.	O	110	797	580	470	8.0	12.3	Y	11.9	Y
		111	809				6.5		6.8	
		Flange pair	810 810				12.4 12.4	Y Y	12.4 12.4	Y Y
			811				15.5	Y	15.5	Y
		112	822				7.4		7.7	
		Flange pair	823 823				13.0 13.0	Y Y	13.1 13.1	Y Y
			824				15.8	Y	16.0	Y
		113	750				7.9		8.0	
		Flange pair	751 751				12.9 12.9	Y Y	12.8 12.8	Y Y
18-in.	O	Main	680	580	470	8.1	5.7		5.8	
			683				5.8		6.0	
			691				5.3		5.8	
			729				5.4		5.3	
			732				5.7		5.4	
			736				5.4		4.7	

[a]See footnate to Table 1.

INTERNAL DISTRIBUTION

1. J. D. Bumgardner
2. S. J. Chang
3-6. R. D. Cheverton
7. D. H. Cook
8. R. A. Crone
9. R. E. Daniels (DOE-ORO)
10. H. L. Debban
11. M. B. Farrar
12. R. E. Hale
13. R. E Henry
14. R. W. Hobbs
15-25. J. R. Inger
26. K. Iskander
27. H. A. Kmieciak
28 M. W. Kohring
29 M. A. Linn
30. R. S. McKeehan
31. L. D. Merryman
32. D. J. Newland
33. L. D. Proctor
34. C. T. Ramsey
35. D. R. Reed (DOE-ORO)
36. J. B. Roberto
37. K. A. Smith
38. L. C. Smith
39. R. M. Stinnett
40. H. R. Vogel
41. RRD-DCC
42. Central Research Library
43. Document Reference Section
44-45. Laboratory Records
46. Laboratory Records (RC)

EXTERNAL DISTRIBUTION

47-48. Office of Scientific and Technical Information, Post Office Box 2, Oak Ridge, TN 37831